This is to certify that the

thesis entitled

The High Silica Rainier Mesa Magma Batches:
Implications on the Origin of Large Volume
Compositionally Zoned Magmatic Systems

presented by

Benjamin Woods Saltoun

has been accepted towards fulfillment
of the requirements for

Masters degree in Geological Sciences

Thomas A. Vogel

Major professor

Date 10/16/95

THE HIGH SILICA RAINIER MESA MAGMA BATCHES: IMPLICATIONS ON THE ORIGIN OF LARGE VOLUME COMPOSITIONALLY ZONED MAGMATIC SYSTEMS

By

Benjamin Woods Saltoun

A THESIS

Submitted to
Michigan State University
in partial fulfillment of the requirements
for the degree of

MASTER OF SCIENCE

Department of Geological Sciences

1995

ABSTRACT

THE HIGH SILICA RAINIER MESA MAGMAS:
IMPLICATIONS ON THE ORIGIN OF LARGE VOLUME
COMPOSITIONALLY ZONED MAGMATIC SYSTEMS

By

Benjamin Woods Saltoun

Chemical heterogeneities occur in many large-volume ash-flow sheets. Most workers have assumed that the high-silica portions of these deposits evolved largely by differentiation processes that occurred within the magma chamber. However, the chemical heterogeneities of glassy pumice fragments within the large volume, Rainier Mesa ash-flow sheet are not consistent with these processes. They occur in two primary chemical groups. A low and high silica group. Additionally, the high-silica group contains two distinct populations; a low-Th and a high-Th population. Geochemical, mineralogical and geothermometry data on the high silica populations confirms the separate nature of these groups. All three magma types were resident in the pre-eruptive Rainier Mesa magma chamber. Yet, major and trace element variations of the high silica magma batches, especially La, Th and Zr, cannot be modeled by differentiation processes that can occur within a single magma body.

This abstract has been cut from its original form to fit the space requirements of the university.

ACKNOWLEDGMENTS

I guarantee that you would not be holding this thesis were it not for the help of two people: Tom Vogel and Kris Huysken. Firstly, I would like to thank my advisor, Tom, for his unmitigated financial, intellectual and moral support throughout the duration of this project. Tom knew when to help me, and he knew when to let me figure it out. I also thank Kris, firstly, for the comradeship and, secondly, for answering my many geology questions.

I would also like to thank my committee members, Bill Cambray, Duncan Sibley and Dave Matty for their willingness to assist in the completion of this study.

TABLE OF CONTENTS

LIST OF TABLES

LIST OF FIGURES

Introduction

The origin of compositionally zoned magma chambers is currently one of the most actively studied fields within igneous petrology. The common occurrence of zoned magma chambers is well documented. de Silva and Wolff (1995) maintain that *in situ* differentiation is almost entirely responsible for any observed major and trace element variations that occur within a zoned magma chamber. Their hypothesis is primarily based on: (1) the observation that smaller volume zoned magmatic systems exhibit extreme compositional zonation (Smith, 1979; Hildreth, 1981; de Silva, 1991), whereas, large volume systems are commonly weakly zoned or homogenous (Whitney and Stormer, 1985; de Silva, 1989a; Best et al., 1989; de Silva and Wolff, 1995); (2) the range of major and trace element variation in zoned magmas which is consistent with crystal fractionation (Michael, 1983; Wolff and Storey, 1984; Wörner and Schmincke, 1984a, b; Cameron and Cameron, 1986); (3) the inference most isotopic variations are the result of magmatic contamination by fluids and/or assimilation of wall rock (Wörner et al., 1985; Palacz and Wolff, 1989; Tegtmeyer and Farmer, 1990) and (4) that calculated zoning times are in general agreement with independent estimates.

Large-volume, compositionally zoned magmatic systems have been observed by many workers (e.g., Dunbar and Hervig, 1992b; Stix and Gordon, 1993; Cambray et al., 1995). However, reasonable *in situ*

differentiation models fail to characterize the chemistry of these systems. Cambray et al. (1995) have recently proposed that compositional zonation in the large volume Rainier Mesa magma system was the result of batch melting. They suggest that chemically distinct magma batches formed at the source area by partial fusion of a protolith; either by heterogeneous melting of a single protolith or simultaneous melting of multiple source areas (Sawyer, 1994). These chemically distinct magma batches were extracted from the source area either sequentially or simultaneously along faults. If different magma batches simultaneously used the same fault conduit, they would remain separate due to viscosity differences (Carrigan and Eichelberger, 1990; Carrigan, 1994). Over time, these chemically distinct magma batches were stored within a dilatant releasing bend and became density stratified to form a compositionally zoned magma chamber. Thus, the chemical variations among the different magma batches are not consistent with *in situ* differentiation mechanisms. However, the variations within a single magma batch could have been the result of *in situ* differentiation or continuous reaction melting (Cambray et al., 1995).

Considering its large compositional range (55 to 76 wt% SiO_2), the Rainier Mesa ash-flow sheet is ideal for the study of large volume zoned magmatic systems. The Rainier Mesa ash-flow sheet represents an 11.6 Ma eruptive event that explosively erupted more than 1200 km^3 of material. Given the compositionally zoned nature of the Rainier Mesa ash-flow sheet,

most workers have assumed that the pre-eruptive Rainier Mesa magma chamber was chemically and thermally zoned. Furthermore, prior studies have determined that the ash-flow sheet is associated in time and place with Basin and Range extension (Byers et al., 1976a; Christiansen et al., 1977; Eaton, 1984).

Mills (1991) extensively studied the geochemistry of the Rainier Mesa ash-flow sheet. His detailed analysis indicated the presence of three compositionally distinct magma batches. Mills (1991) observed that the Rainier Mesa ash-flow sheet is composed primarily of two main groups of magma: a low silica batch (55 to 72 wt% SiO_2) and a high silica group (72 to 76 wt% SiO_2). The high silica group is, furthermore, composed of two separate and distinct magma batches: high-Th/Nb ratio magma and a low-Th/Nb ratio magma. Also, the high silica group comprises approximately 90% of the total volume of the Rainier Mesa ash-flow sheet (~1080 km^3) (Mills, 1991).

The purpose of this study is, firstly, to confirm the existence of the high and low Th/Nb ratio magmas observed by Mills (1991). Secondly, to determine if the high and low Th/Nb ratio magma batches are related by *in situ* differentiation; and finally,at the same time, test the work of Cambray et al. (1995) and de Silva and Wolff (1995).

In summary, de Silva and Wolff (1995) suggest that *in situ* differentiation cannot produce the significant chemical and thermal

zonations observed in many large volume systems. Consistent with this suggestion is the Cambray et al. (1995) proposal that batch melting is the mechanism by which the large volume compositionally zoned Rainier Mesa system formed. The purpose of this research is to determine the petrogenic relationship that exists between the high silica Rainier Mesa magma batches.

Geologic Setting

The Rainier Mesa Tuff is part of the Southwest Nevada Volcanic Field (SWNVF), and is located within the south-central Basin and Range Province (Fig. 1). This area is characterized by extensive volcanism that occurred from 15.25 Ma to 7.5 Ma (Sawyer, 1994). Within the SWNVF are four large volume compositionally zoned ash-flow sheets, one of which is the Rainier Mesa ash-flow sheet. The eruption of both the Rainier Mesa (1200 km^3) and Ammonia Tanks (900km^3) ash-flow sheets resulted in the development of the large Timber Mountain caldera complex. The Timber Mountain Caldera complex was uplifted 1200 m after the eruption of the Ammonia Tank Tuff. This uplift resulted in the formation of the present day Timber Mountain (Christiansen, et al., 1977).

Structurally, the Timber Mountain Caldera complex is associated with the Walker Lane Belt (Carr, 1990). The Walker Lane belt is a northwest trending fault zone composed of right and left lateral detachment faults and northwest trending structural blocks (Stewart, 1988; Scott, 1990). Furthermore, geophysical evidence indicates that SWNVF overlies an extensional pull-apart basin that coincides to a right-step in the Walker Lane belt (Carr, 1990).

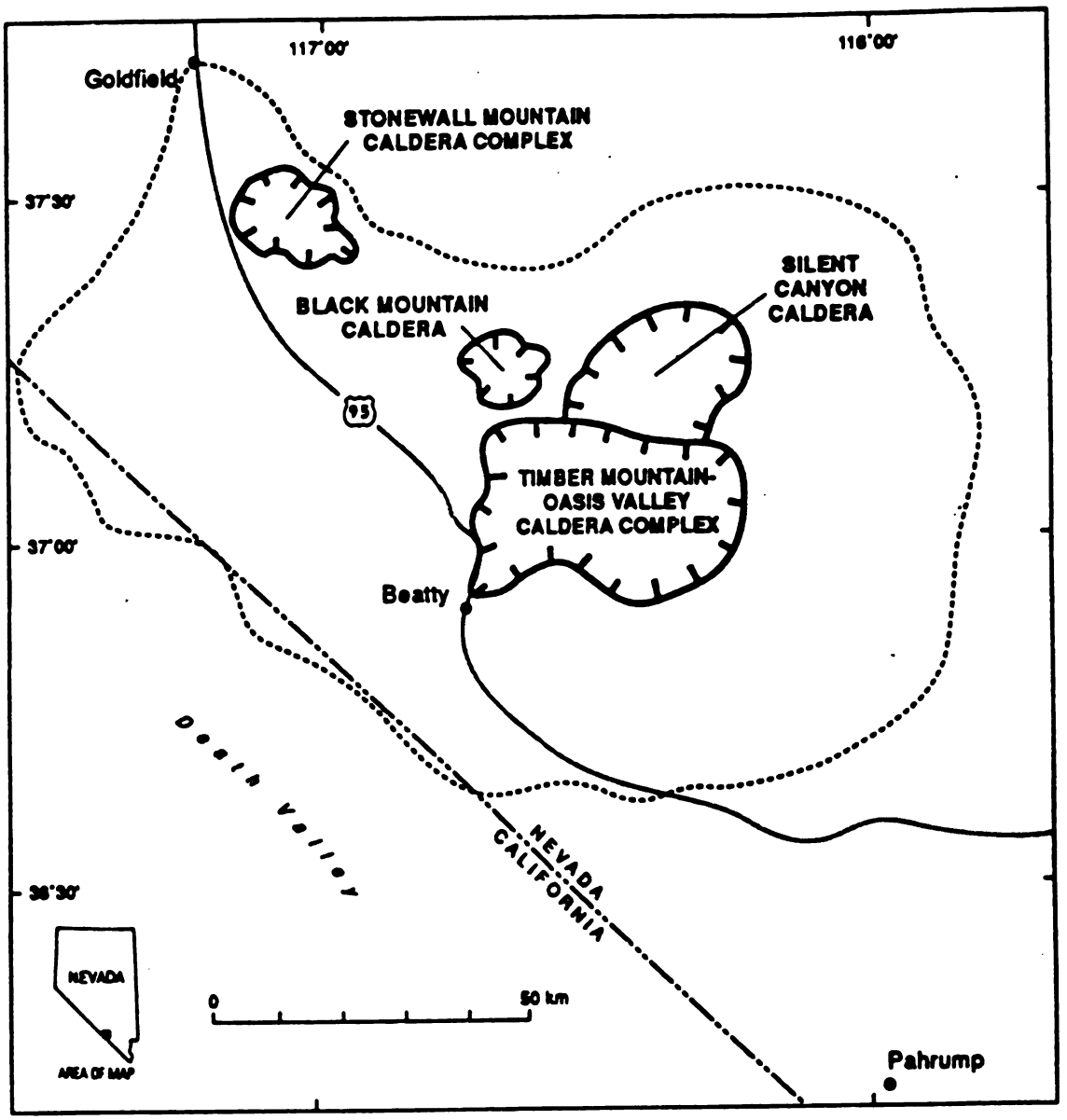

Figure 1. Location map of the Southwest Nevada Volcanic Field. The stippled line delineates the spatial extent of the Timber Mountain Group (after Carr et al., 1984; Noble et al., 1984; and Vogel et al., 1987).

Sampling Procedure

Glassy pumice fragments from the high silica portion of the Rainier Mesa ash-flow sheet were analyzed for major and trace elements using XRF and INAA techniques (see appendix A). Because glassy pumice fragments represent pockets of solidified magma that were instantaneously erupted from a single vent (Flood, 1989), they provide a better indication of processes that may have occurred within the magma than whole ash-flow tuff samples (Hildreth and Mahood, 1985; Flood et al., 1989; Schuraytz et al., 1989; Vogel et al., 1989; Mills, 1991; Huysken and Vogel, 1993). Conversely, whole ash-flow tuff samples represent an average composition of all material being deposited over a given period of time at a given location. Hence, glassy pumice fragments provides the most accurate representation of actual magma compositions, minus lost volatiles, at the moment of eruption (Flood, 1987).

Rainier Mesa Geochemistry

Mills (1991) extensively evaluated the compositional and chemical spectrum of the Rainier Mesa ash-flow sheet. Glassy pumice sample compositions were classified by Mills (1991) using the Total Alkali-Silica (TAS) classification system of Le Bas et al. (1986). The TAS diagram indicates that the entire Rainier Mesa ash-flow sheet compositionally ranges from trachyandesite to rhyolite (Fig. 2) (Mills, 1991). It has been noted that mobilization of alkalis can occur by secondary hydration of glass (Aramaki and Lipman, 1965; Lipman, 1965; Noble, 1967). Hence, alkali mobilization can skew classification based on the TAS method (Le Bas et al., 1986; Irvine and Barager, 1971). Mills (1991) observed that alkali mobilization within the Rainier Mesa ash-flow sheet is minimal based on the small variance of the alkali data.

As observed by Mills (1991) and Cambray et al. (1995) the most remarkable characteristic of the Rainier Mesa ash-flow sheet is a large silica gap between 71 and 73 wt% SiO_2 (Fig. 3). This silica gap demarcates the existence of the two main trends within the Rainier Mesa ash-flow sheet. The low silica trend occurs between 57 and 71 wt% SiO_2 and the high silica trend occurs between 73 and 78 wt% SiO_2. The variation diagrams produced by plotting Zr and La versus Th provide the best picture of the distinct nature of these two trends (Fig. 4) (Mills, 1991). Furthermore, Figure 4

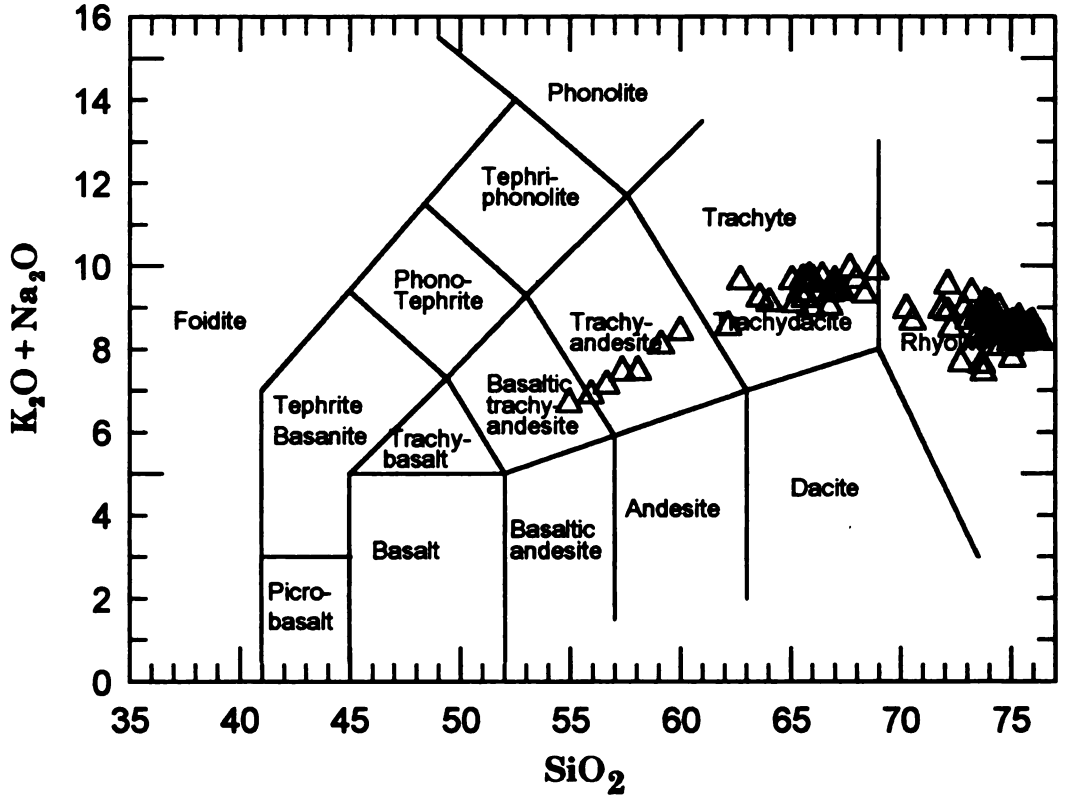

Figure 2. Total Alkali-Silica classification diagram. The entire Rainier Mesa Tuff is plotted. Includes data from Mills (1991).

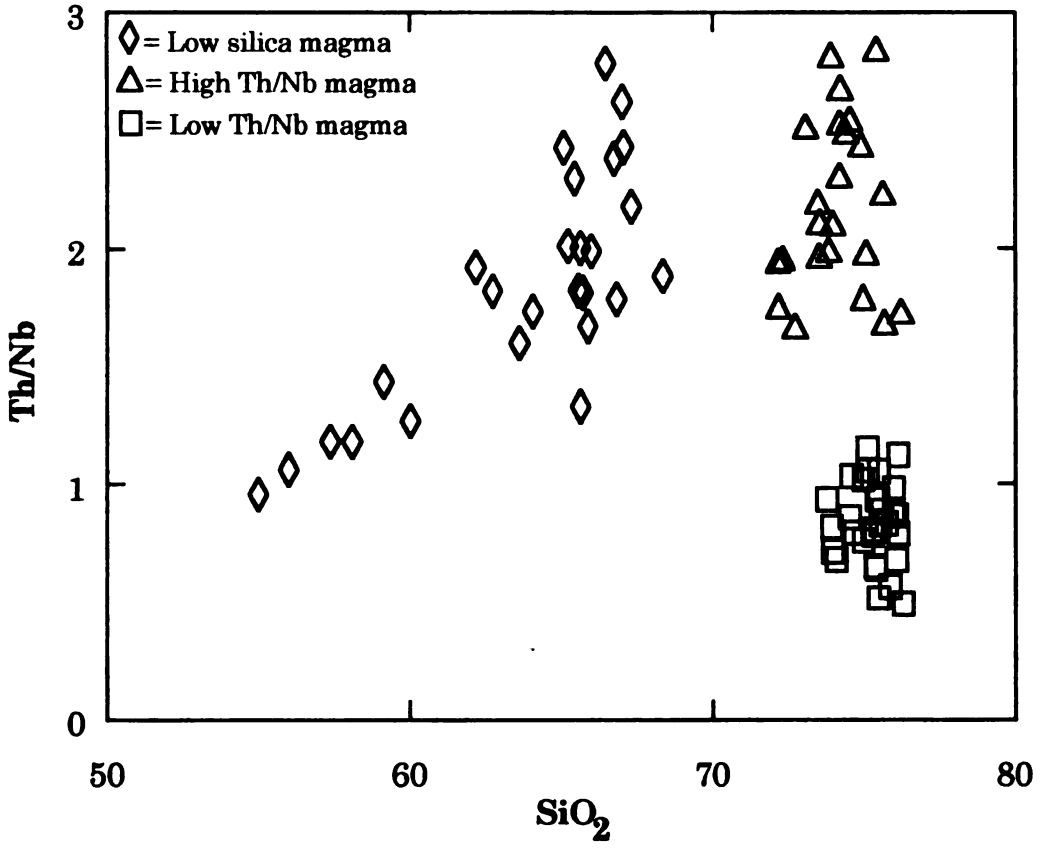

Figure 3. SiO_2 vs Th/Nb. This diagram shows the two primary magma groups of the Rainier Mesa Tuff. The high and low silica groups are seperated by a SiO_2 gap at approximately 70 wt%.

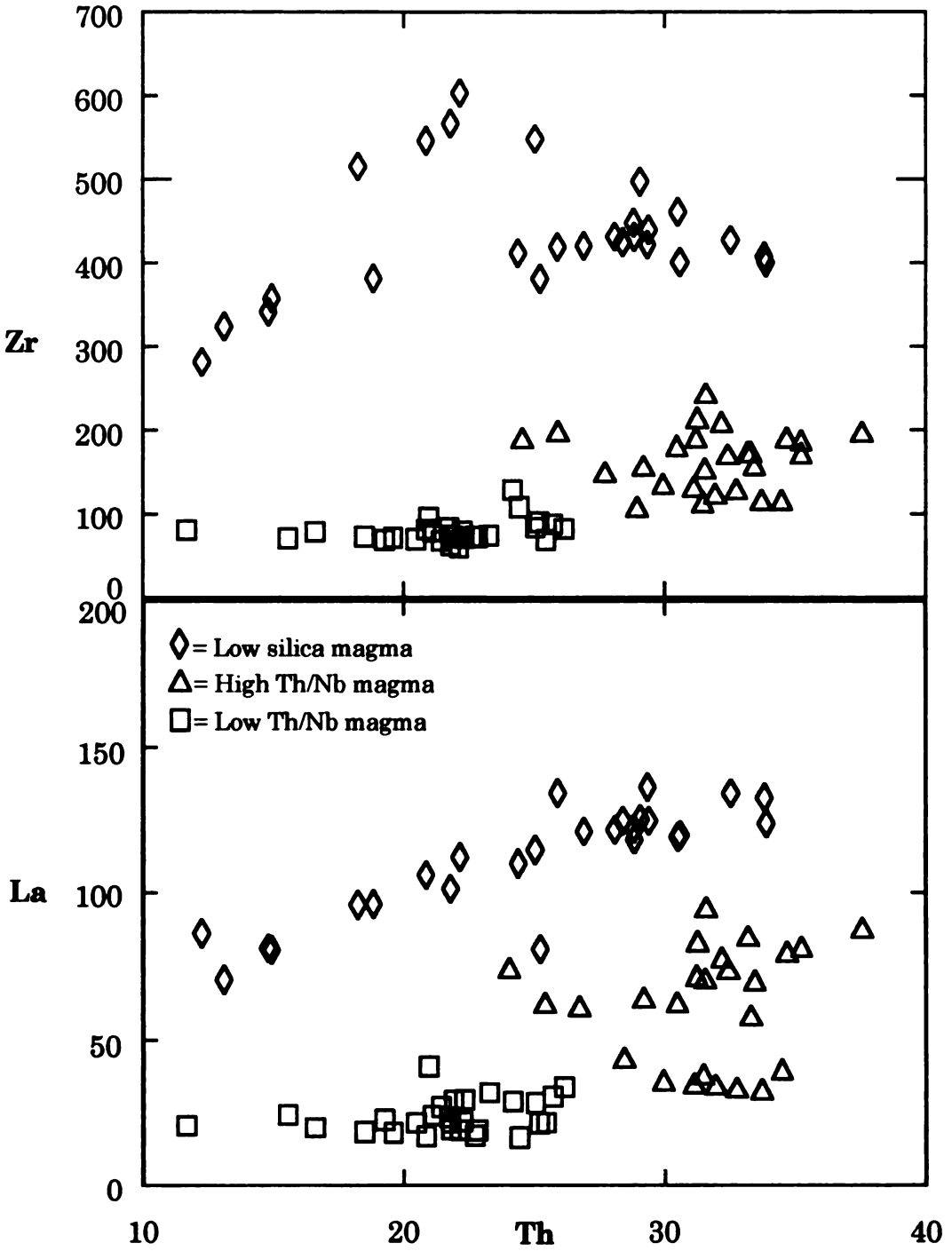

Figure 4. Th vs. Zr and La. The absence of differentiation pathways indicates that *in situ* differentiation cannot petrogenically relate the three Rainier Mesa magma types (after Cambray et al., 1995).

clearly shows that Zr and La versus Th variations between the low silica trend and high silica trend cannot be produced by reasonable *in situ* differentiation processes such as crystal fractionation or magma mixing. This conclusion is based on the observation that there are no differentiation pathways between the high silica and low silica trends for these elements (Cambray et al., 1995).

Mills (1991) originally identified two separate high silica Rainier Mesa magma types based on Th and Nb; a high Th/Nb ratio magma batch and a low Th/Nb ratio magma batch (Fig. 5). These two high silica magma types are also easily distinguished by the Zr and La versus Th, and SiO_2 versus Th/Nb variation diagrams (Fig. 4). Additionally, Figure 4 also indicates that reasonable *in situ* differentiation processes cannot petrogenically relate the high and low Th/Nb magma types to one another. Cambray et al. (1995) also noted that there is no geochemical overlap between the high and low-Th magmas; as exhibited by variation diagrams of major and trace elements versus Th/Nb (Figs. 6 and 7). The chemically distinct nature of the high and low-Th magmas in conjunction with the lack of reasonable differentiation pathways suggest that these magmas are genetically unrelated (Cambray et al., 1995). Furthermore, step-wise major element and trace element modeling of the high and low-Th/Nb magmas was completed for this study. This modeling quantitatively determined if realistic *in situ* differentiation

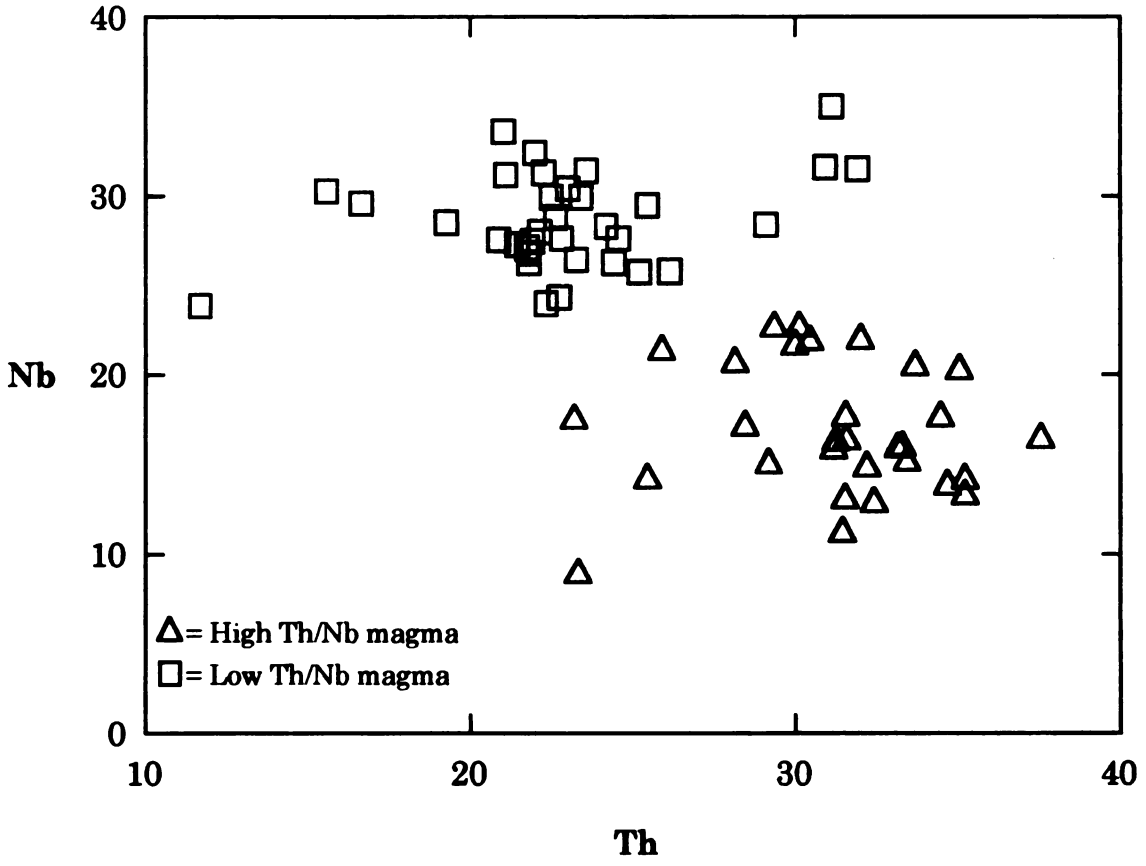

Figure 5. Th vs. Nb for the high silica Rainier Mesa Tuff.

Figure 6. Th/Nb versus selected major element oxides (after Cambray et al., 1995).

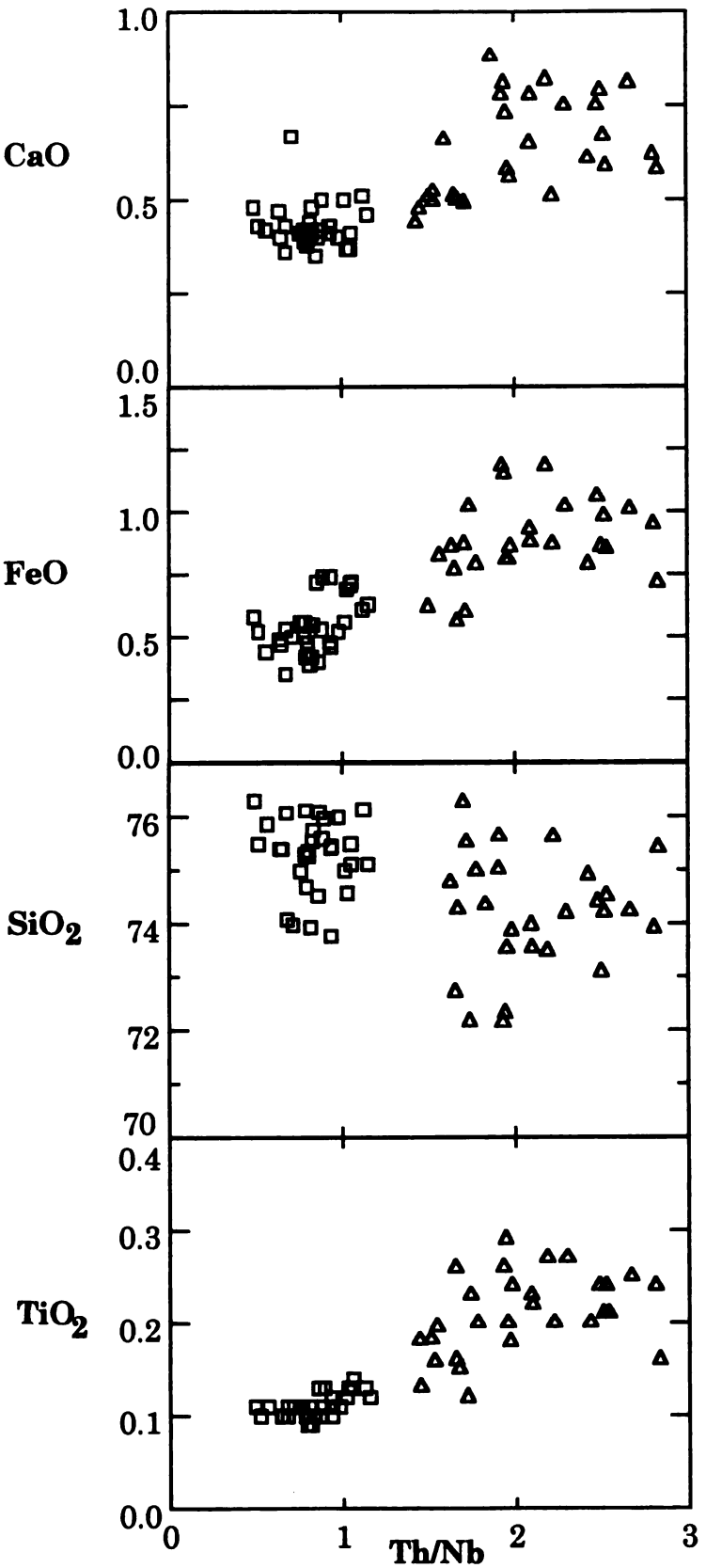

□= Low Th/Nb magma △= High Th/Nb magma

Figure 7. Th/Nb versus selected trace element ratios (after Cambray et al., 1995).

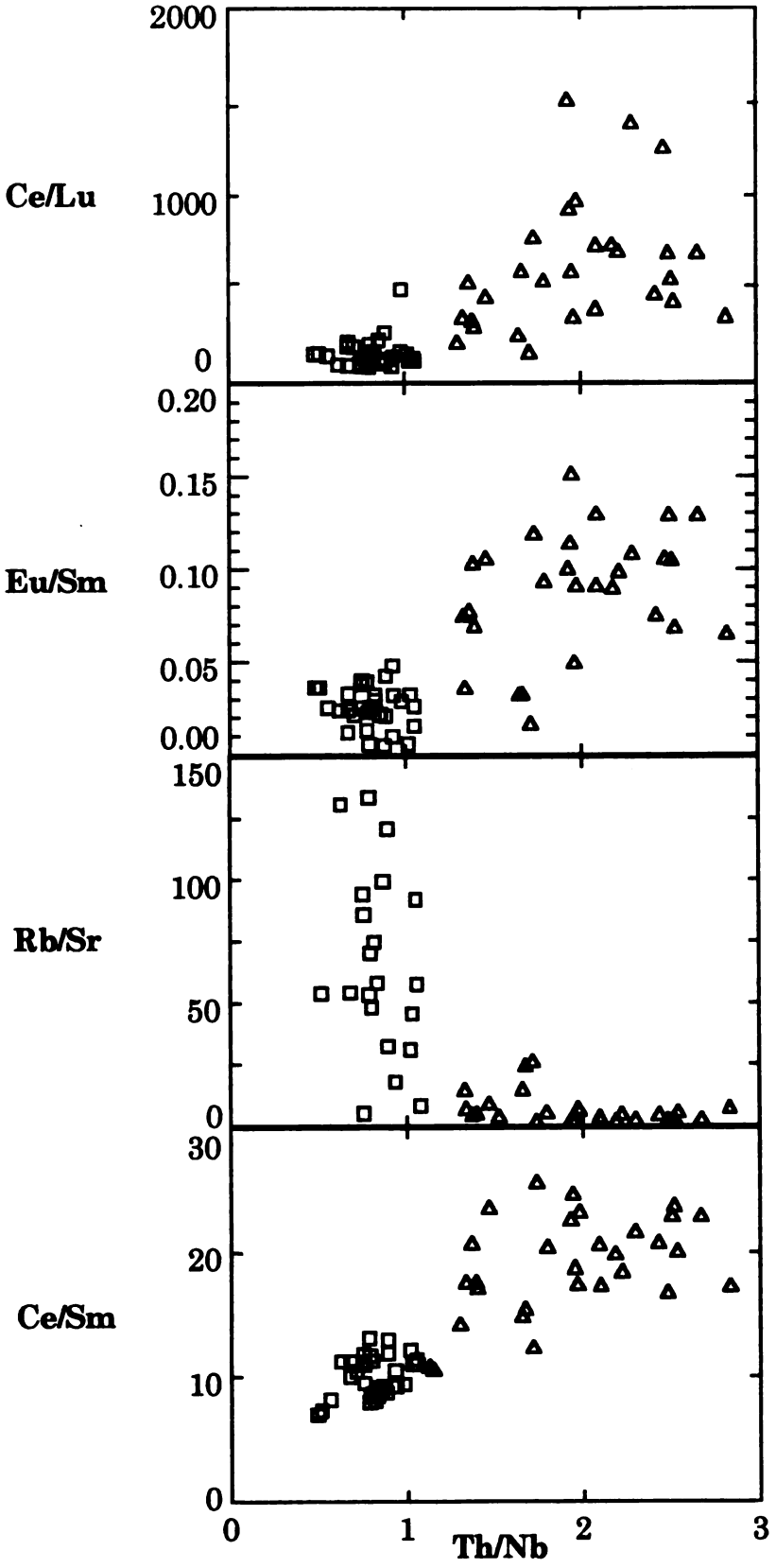
Ce/Lu
2000
1000
0
Eu/Sm
0.20
0.15
0.10
0.05
0.00
Rb/Sr
150
100
50
0
Ce/Sm
30
20
10
0
0
1
2
3
Th/Nb
□= Low Th/Nb magma △= High Th/Nb magma

models could petrogenically relate these magmas. All models for Raleigh crystal fractionation, magma mixing and assimilation fractional crystallization fail to accurately predict the observed geochemistry of the high and low-Th/Nb magmas. For the remainder of this paper, the high and low Th/Nb ratio magmas will be referred to simply as the high-Th magma or the low-Th magma.

In an effort to confirm the existence of high and low-Th magmas first observed by Mills (1991) and characterized by Cambray et al. (1995), additional analyses of new high silica glassy pumice fragments from the Rainier Mesa ash-flow sheet was completed. A primary goal of this research was to determine if these distinct populations would be better defined by additional sampling of the high silica compositions. This analysis has confirmed the existence of the high and low-Th magmas. New geochemical data of the high and low-Th magmas also exhibit no geochemical overlap, as shown by variation diagrams of selected major and trace elements versus Th/Nb (Figs. 8 and 9). Figures 8 and 9 demonstrate that the high and low-Th magmas are distinct with respect to both major and trace elements. Note that new geochemical analysis for the high and low-Th magmas are consistent with Mills' (1991) analysis. This data indicates that Mills' (1991) XRF and INAA whole-pumice analysis are reproducable.

Figure 8. Th/Nb versus selected major element oxides; includes symbols that depict new whole-pumice geochemistry for the high and low-Th magma batches.

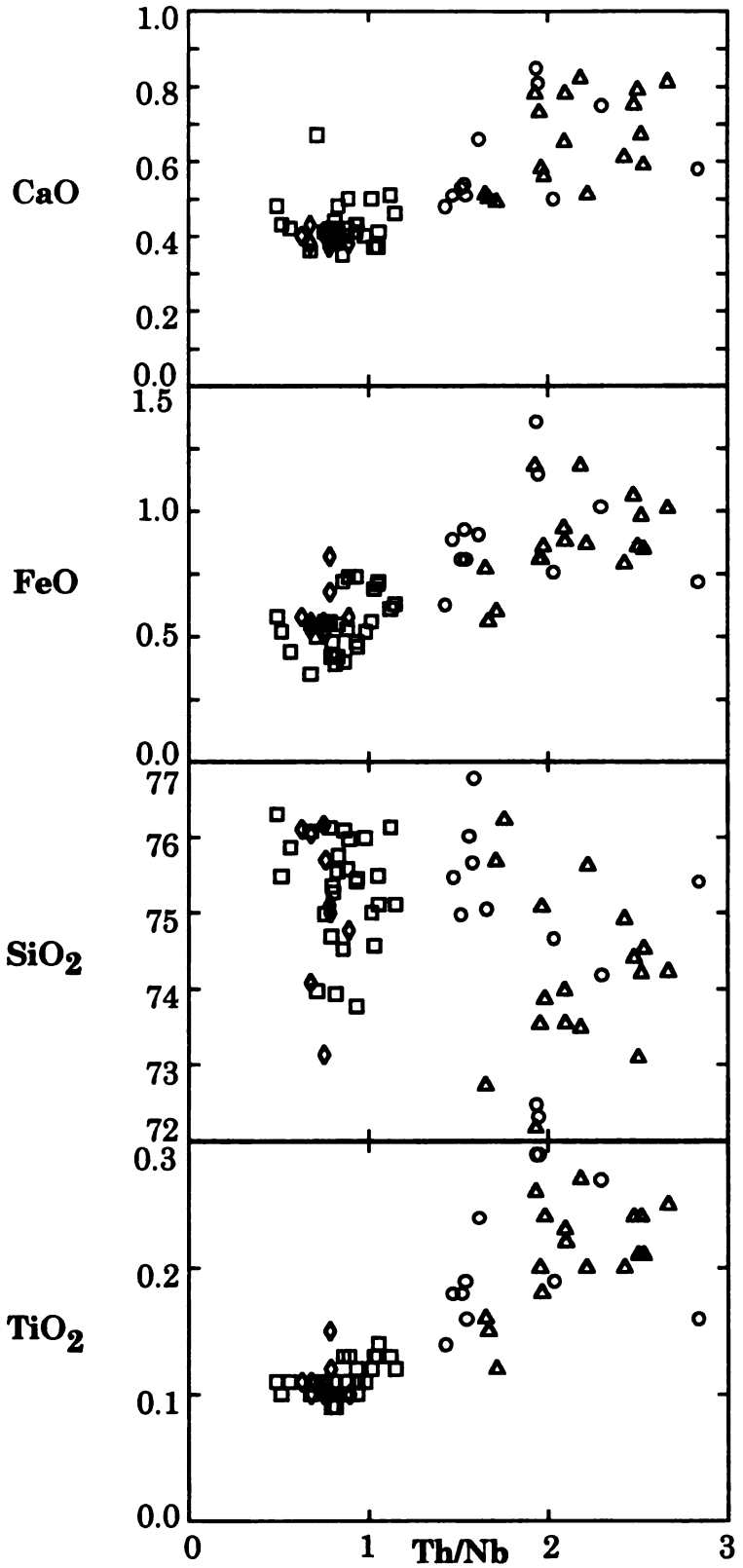

□= Low Th/Nb magma △= High Th/Nb magma

◊= New Low Th/Nb magma ○= New High Th/Nb magma

Figure 9. Th/Nb versus selected trace element ratios; includes symbols that depict new whole-pumice geochemistry for the high and low-Th magma batches.

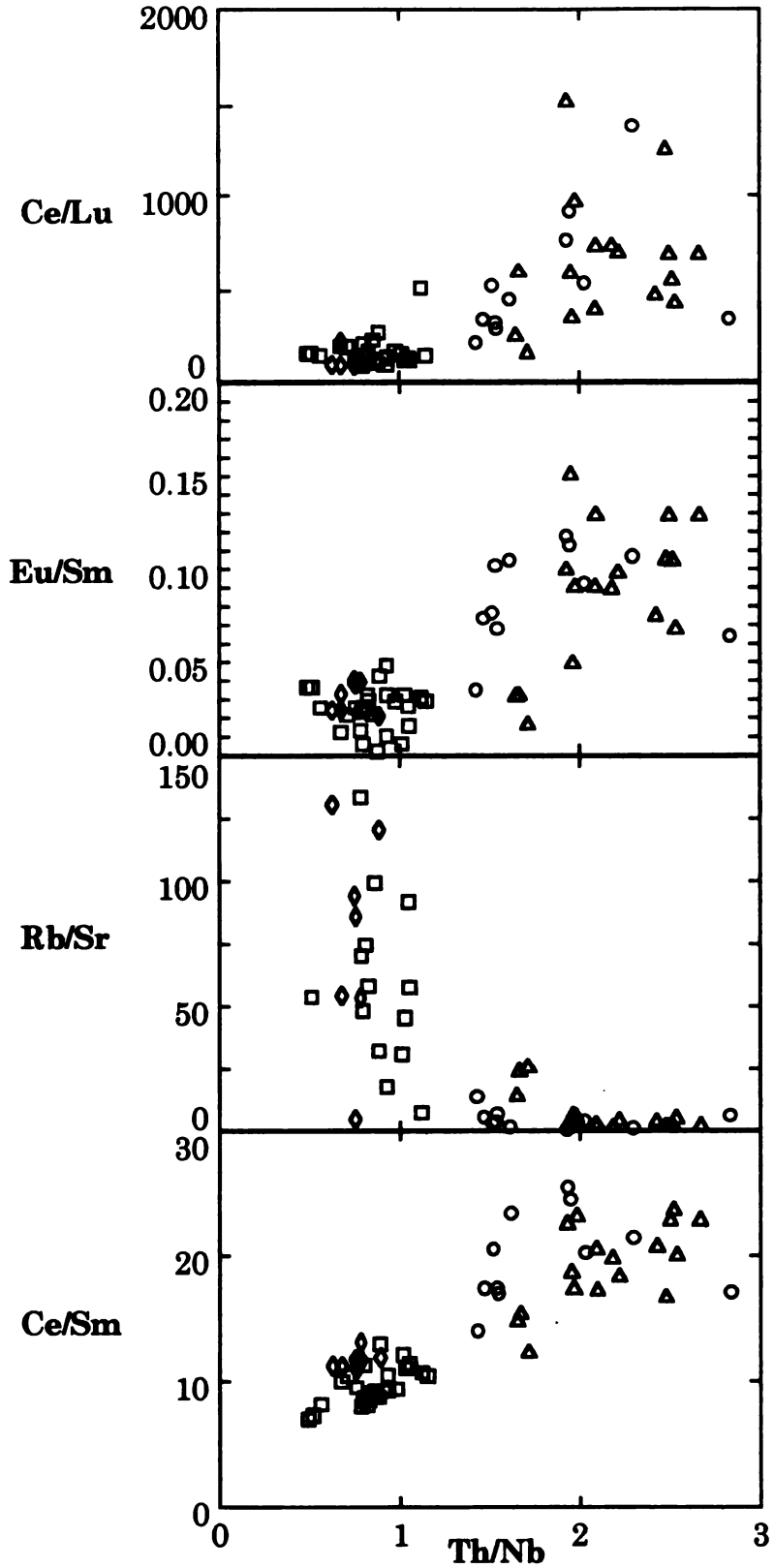

□= Low Th/Nb magma △= High Th/Nb magma

◊= New Low Th/Nb magma ○= New High Th/Nb magma

Mineral Assemblage chemistries of the high and low-Th magmas

In order to determine the relationship between the high and low-Th magmas, a complete electron microprobe study of the chemical compositions of the mineral assemblage was completed. The two magma types contain different assemblages with distinct compositions. Both the high and low-Th magmas contain biotite, ilmenite, magnetite, alkali feldspar and plagioclase feldspar. However, pyroxene and amphibole occur only in the high-Th magma.

Ilmenite

The chemistry of ilmenite for both the high and low-Th magmas are different. Ilmenite grains from the high-Th magma have FeO compositions which range from 49 to 55 wt%. TiO_2 compositions range from 36.4 to 40 wt%. Whereas, FeO compositions in ilmenite for the low-Th magma range from 45 to 49 wt% and TiO_2 compositions range from 42 to 45 wt% (Fig. 10a). Additionally, MgO and MnO concentrations in ilmenite are different for the high and low-Th magmas; the high-Th magma has higher MgO and lower MnO than the low-Th magma (Fig. 10b).

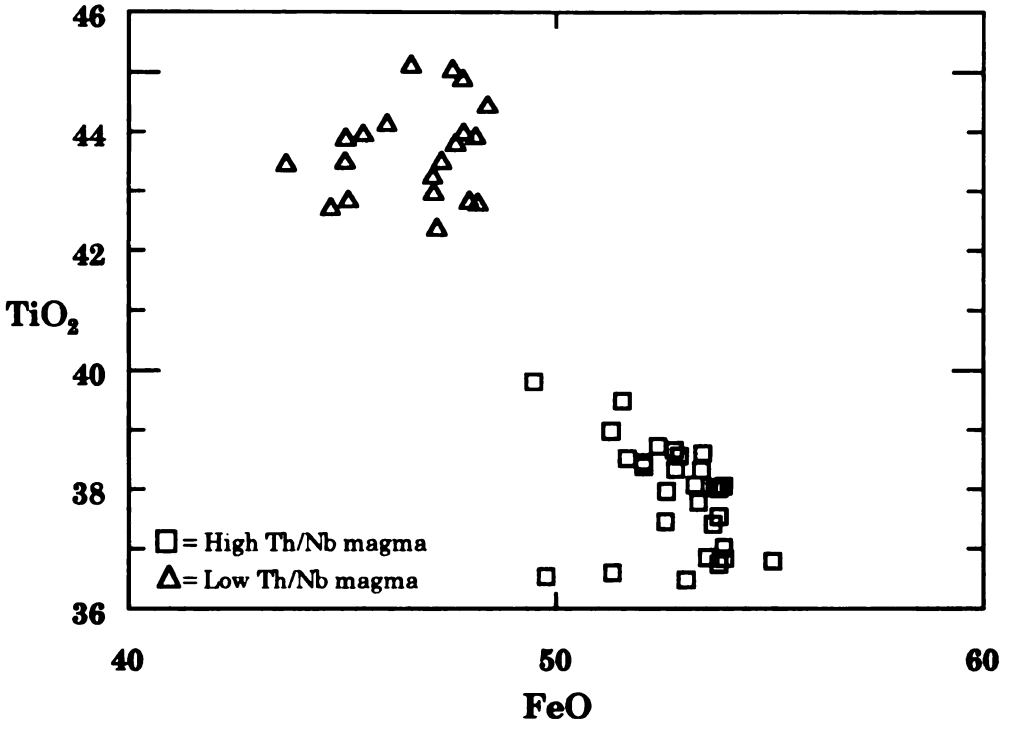

Figure 10a. FeO versus TiO_2 variation diagram for ilmenite compositions of the high and low-Th magma batches.

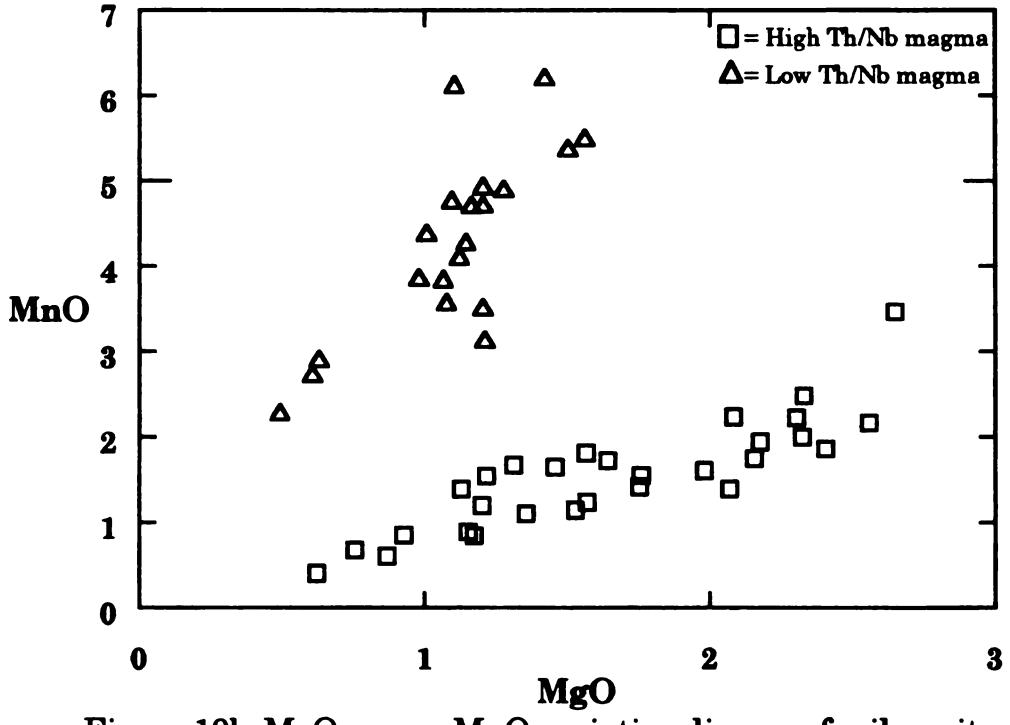

Figure 10b. MgO versus MnO variation diagram for ilmenite compositions of the high and low-Th magma batches

Magnetite

The composition of magnetite for the high and low-Th magmas are different. The TiO_2 content of the magnetite from the low-Th magma range from 4.5 to 5.5 wt% and FeO concentrations range from 83 to 85 wt%. In contrast, the TiO_2 compositions of magnetite from the high-Th magma range from 5.5 to 7.3 wt% and FeO compositions range from 77 to 84 wt% (Fig. 11a). The MgO and MnO content of the magnetite are different among the high and low-Th magmas; this variation is similar to that of ilmenite. The high-Th magnetite grains have higher MgO and smaller MnO concentrations than the low-Th magnetite grains (Fig. 11b).

Biotite

Biotite is abundant in the high and low-Th magmas; and their compositions are distinct in both the high and low-Th magmas. The Al_2O_3 compositions of the biotite grains in the low-Th magma range from 11.7 to 13.5 wt% and TiO_2 contents range from 3 to 3.7 wt%. The high-Th biotites have a much larger chemical variation. The Al_2O_3 contents of biotite in the high-Th magma range from 12 to 18.5 wt% and TiO_2 contents range from 4.1 to 6.1 wt% (Fig. 12a).

The SiO_2 and MnO contents in biotite are different between the high and low-Th magmas. The SiO_2 content in biotite of the low-Th magmas

range from 35.5 to 40.7 wt%. Conversely the SiO_2 content in biotites of the high-Th magmas range from 31 and 38.4 wt%. Additionally, the low-Th biotites have higher MnO concentrations than the high-Th biotites. The MnO contents in biotite of the low-Th magma range from 0.5 to 0.7 wt%, while the MnO contents in biotites of the high-Th magma range from 0.3 to 0.6 wt% (Fig. 12b).

Feldspar

The plagioclase compositions are different between the high and low-Th magmas. The average plagioclase composition in the low-Th magma is An_{14}, whereas the average plagioclase composition in the high-Th magma is An_{21} (Fig. 13). Almost all plagioclase feldspars are compositionally homogenous from the center of the grain to the edge, with very little compositional variation among the plagioclase of each magma batch. However, approximately 5% of the plagioclase grain are compositionally zoned. These ubiquitous grains are clearly observable in Figure 13 and have Ca-rich cores that gradationally evolve to Na-rich edges. Unlike the compositions of magnetite, ilmenite, biotite and plagioclase, the composition of the alkali feldspar grains for both the high and low-Th magmas are indistinguishable from one another within error of analysis (Fig. 13).

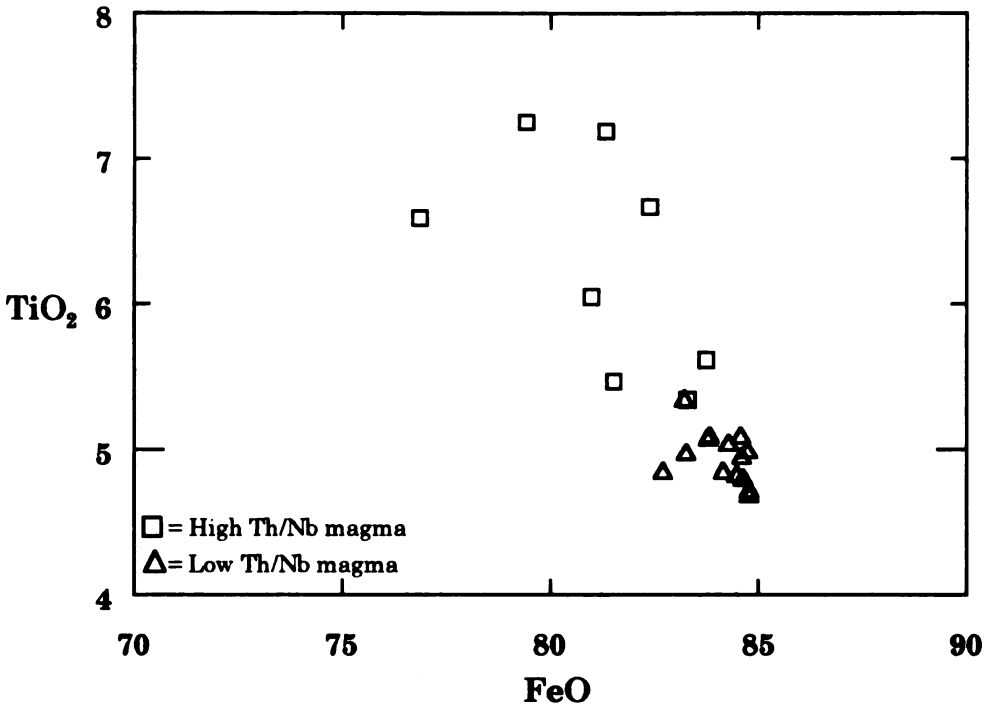

Figure 11a. FeO versus TiO2 variation diagram for magnetite compositions of the high and low-Th magma batches.

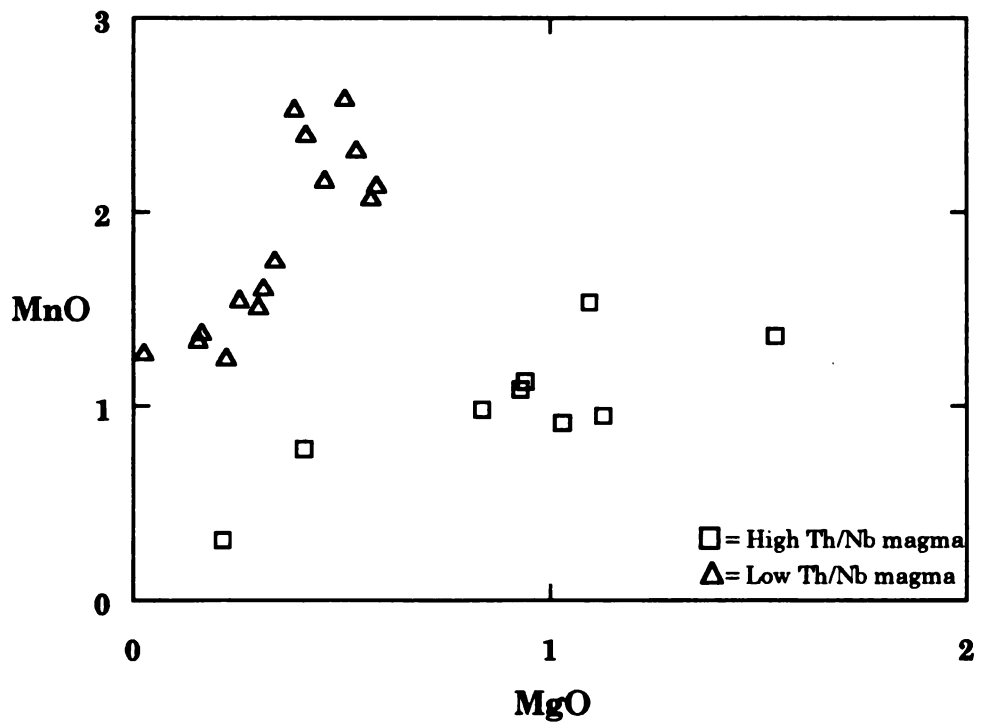

Figure 11b. MgO versus MnO variation diagram for magnetite compositions of the high and low-Th magma batches.

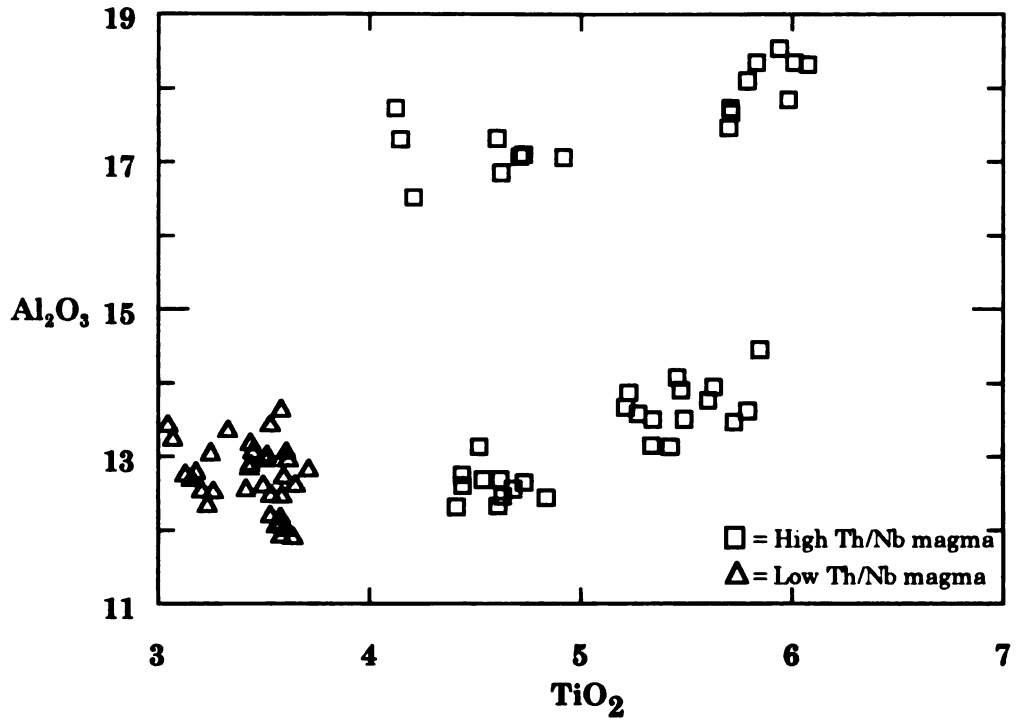

Figure 12a. TiO_2 versus Al_2O_3 variation diagram for biotite compositions of the high and low-Th magma batches.

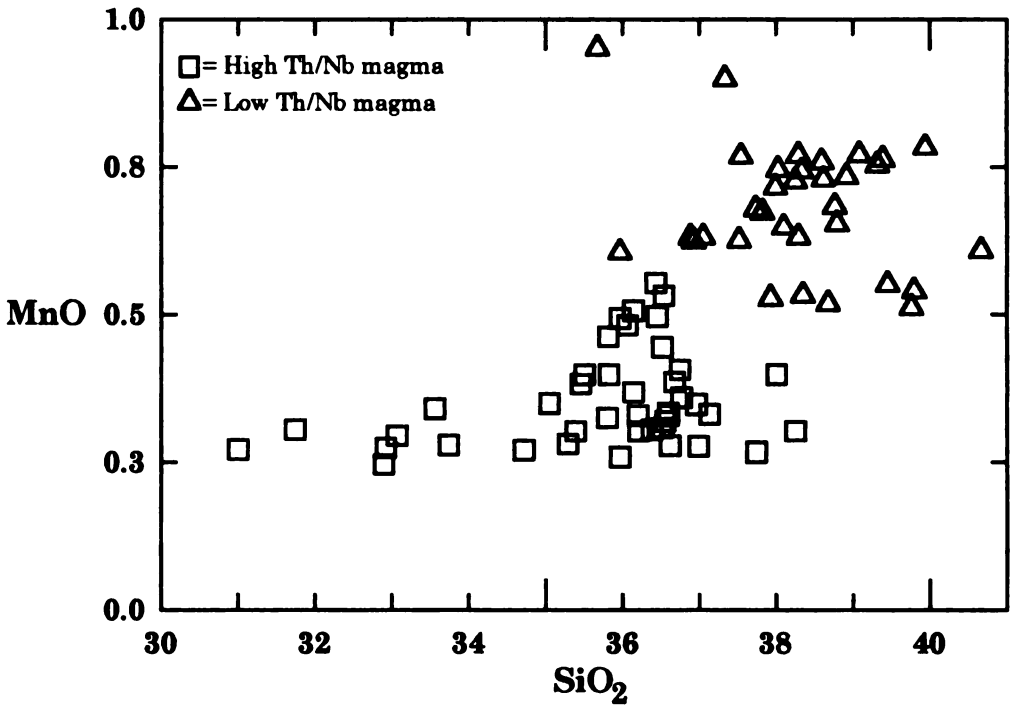

Figure 12b. SiO2 versus MnO variation diagram for biotite compositions of the high and low-Th magma batches.

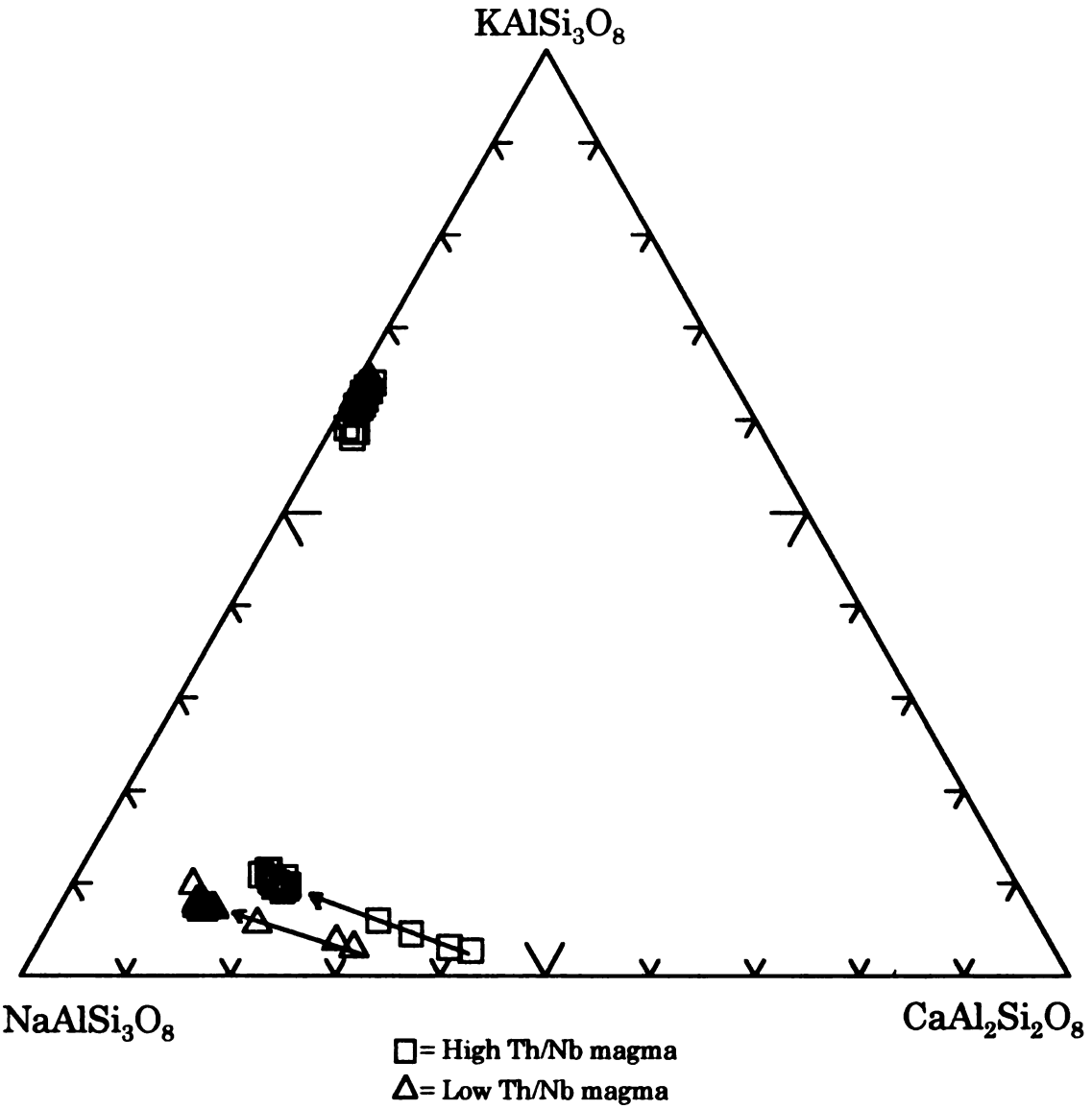

Figure 13. Ternary feldspar diagram showing plagioclase and alkali-feldspar compositions. The arrows indicate inferred paths of magmatic evolution.

Geothermometry

Fe-Ti Oxide Geothermometry

Electron microprobe analysis of ilmenite and magnetite allowed for the calculation of pre-eruptive magma temperatures and oxygen fugacities. Calculation of ulvospinel and hematite compositional parameters were completed by the program OXPROJWT (Anderson et al., 1993) for all magnetite grains. Ulvospinel and hematite compositions for all grains from a single pumice fragment were statistically analyzed to determine population distribution and mean composition. Mean compositional parameters for magnetite and ilmenite pairs were then inputted into the Turbo Pascal program QUIIF 4.1 (Anderson et al., 1993), which provided Fe-Ti oxide geothermometry and oxygen fugacity data. Traditionally, Fe-Ti oxide thermometry data is based only on equilibrium between Fe and Ti. QUIIF 4.1 is a versatile program that will calculate Fe-Ti oxide thermometry based on equilibrium between Fe, Mn, Mg, and Ti, which provides better temperature resolution than Fe and Ti alone (Anderson et al., 1993). The low Th magma has an average value of 716 °C and the high-Th magma has an average value of 814 °C (Fig. 14) (Table 1).

Mills (1991) concluded that the high silica Rainier Mesa had an average temperature of 755 °C. His Fe-Ti oxide thermometry data was based only on Fe and Ti equilibrium. Furthermore, the 755 °C temperature

Table 1. Fe-Ti oxide geothermometry data for the high and low magma batches.

descrip.	SiO_2	Th/Nb	Temp°C
R18-15	73.13	0.75	723
R18-6	75.00	0.79	708
R23-7	72.48	1.74	810
R26-14	74.67	1.79	818
R11-7	74.07	0.68	735
R18-2	72.70	1.65	787
R18-16	75.40	2.83	801

Mills (1991) calculated reflects his treatment of the high silica magma batches as a single magma. Using QUIIF 4.1 (Anderson et al., 1993), Vogel (1995, unpublished data) recalculated Fe-Ti oxide temperatures for the entire Rainier Mesa based on Mills' (1991) magnetite and ilmenite data. Vogel (1995, unpublished data) determined that the high-Th magma had an average temperature of 789 °C and the low-Th magma had a temperature of 735 °C. This recalculated thermometry data is based only on three samples; one low-Th sample and two high-Th samples. This thermometry data is presented because it indicates that the high-Th magma had a higher temperature than the low-Th magma; and hence supports the findings of this study.

Ternary-Feldspar Thermometry

The coexistence of sanidine and plagioclase in many of the high and low-Th pumice fragments allows for the determination of geothermometric data. Ternary-feldspar temperatures are constrained by equilibrium among the orthoclase, albite and anorthite components of these coexisting feldspars. Initially, the orthoclase, albite and anorthite components were each calculated from each feldspar grain edge analysis. Descriptive statistics then determined the mean plagioclase and sanidine compositions for each sample

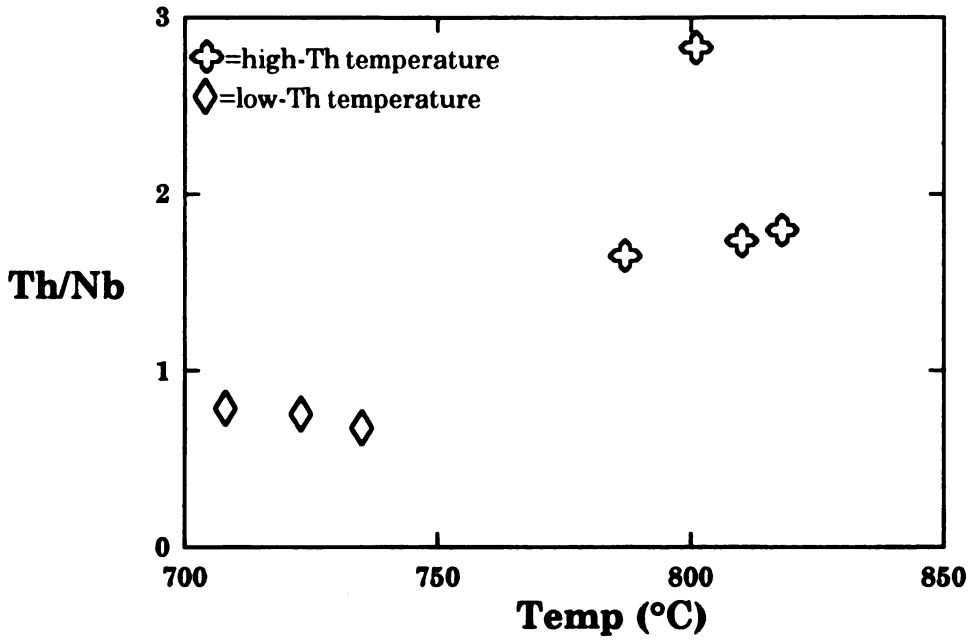

Figure 14. Fe-Ti oxide temperature distribution among the high and low-Th magma batches.

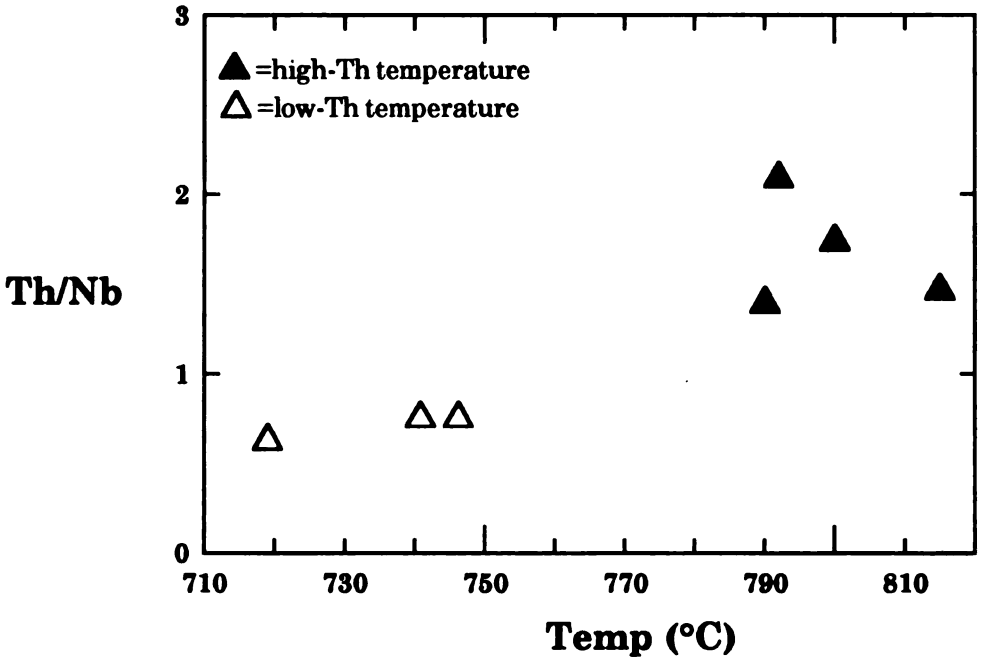

Figure 15. Ternary-feldspar temperature distribution among the high and low-Th magma batches.

Table 2. Mean compositions of coexisting feldspar pairs for the high and low-Th magma batches. Ks denotes alkali-feldspar compositions. Pl denotes plagioclase feldspar compositions.

Sample	An	Ab	Or	Cn
R23-7 ks	0.014	0.368	0.617	0.0003
R23-7 pl	0.189	0.716	0.095	0
R23-8 ks	0.014	0.377	0.609	0
R23-8 pl	0.206	0.714	0.080	7E-05
R23-4 ks	0.012	0.383	0.597	0.0002
R23-4 pl	0.310	0.630	0.059	0.0012
R18-14 ks	0.011	0.350	0.639	0
R18-14 pl	0.148	0.780	0.072	0.0009
R26-19 ks	0.016	0.369	0.614	0.0017
R26-19 pl	0.212	0.715	0.073	0
R18-9 ks	0.008	0.366	0.623	0.0029
R18-9 pl	0.136	0.787	0.078	0
R18-15 ks	0.007	0.360	0.633	0
R18-15 pl	0.129	0.794	0.076	0

(Table 2). Using the mean coexisting feldspar compositions, temperatures were calculated by the Fuhrman and Lindsley (1988) feldspar thermometry model in the SOLVCALC (Wen and Nekvasil, 1994) program.

The ternary-feldspar thermometer is pressure dependent. Typically, this thermometer predicts an increase of 18 °C for every 1kbar increase in pressure (Stormer, 1975; Brown and Parson, 1981). However, ternary-feldspar modeling of the high and low-Th magmas at various pressures did not produce significant temperature variations. Mills (1991) used the quartz-amphibole geobarometry technique to determine that the best pressure estimate for the Rainier Mesa magmatic system is 4.2 kbars. As such, a pressure constant of 4.2 kbars for the feldspar thermometry calculations was used for this study. The low-Th magma has feldspar temperatures which range from 712 to 747 °C and has a mean temperature of 726 °C. The high-Th magma has feldspar temperatures which range from 790 to 815 °C and has a mean temperature of 799 °C (Fig. 15).

Discussion

Background

The occurrence of compositionally zoned magma chambers is not an uncommon phenomena and, subsequently, has been the focus of much research. Yet the physical processes controlling the development of these features remain enigmatic. Many workers have regarded *in situ* differentiation processes as the likely mechanism for the origin of compositionally zoned magma chambers. For example, de Silva and Wolff (1995) stipulate that efficiency of any *in situ* differentiation mechanism ultimately depends on convective fractionation at the vertical chamber wall.

Furthermore, de Silva and Wolff (1995) discuss the relationship between zonation times, volume of magma and chamber shape. Thermal, mechanical and volumetric restrictions require that small volume magma chambers have a column-like chamber shape; whereas, larger volume magmatic systems require a sill or coin-like chamber geometry (de Silva and Wolff, 1995). de Silva and Wolff (1995) suggest there is an inverse relationship between volume of magma and the magnitude of compositional zonation. This conclusion is based, partially, on the observations of Smith (1979), Hildrith (1981) and de Silva (1991). Hence, they maintain that significant magmatic zonation due to *in situ* differentiation can only occur in

small to intermediate volume systems. In large volume magmatic systems, *in situ* differentiation mechanisms cannot produce significant compositional zonation.

The pre-eruptive Rainier Mesa magma chamber was, without question, a large volume compositionally zoned magmatic system. In concordance with the observations of de Silva and Wolff (1995), Cambray et al. (1995) have proposed that the compositional spectrum observed in the Rainier Mesa Tuff cannot be the result of *in situ* differentiation mechanisms. This observation is best illustrated by the Zr and La versus Th variation diagrams (Fig. 4). As previously mentioned, these diagrams illustrate that *in situ* differentiation processes cannot relate the three distinct Rainier Mesa magma types. There are no reasonable differentiation pathways among the magma batches (Cambray et al., 1995). The variation diagrams led Cambray et al. (1995) to propose that the chemistry of the three magma types was controlled by batch melting processes at the source area(s).

The models of de Silva and Wolff (1995) and Cambray et al. (1995) are mutually supporting. Both models conclude that *in situ* differentiation cannot produce large volume compositionally zoned magmas. The Batch Emplacement model of Cambray et al. (1995) was tested by: (1) determining if the magma batches first observed by Mills (1991) are real by better defining the chemistry of the system; and (2) characterizing the petrogenetic

relationship between the high and low-Th magma types. It has been determined the compositionally distinct high and low-Th magma batches observed by Mills (1991) are real. Additionally, it has been determined that these magma batches are compositionally distinct and cannot be petrogenically related by *in situ* differentiation.

Confirmation of the existence of the high and low-Th magma batches

Using mineral and whole-pumice geochemistry in conjunction with geothermometry, the existence of the high and low-Th magma batches has been confirmed. All geochemistry, both whole-pumice and mineral, indicates separate and distinct compositions for the high and low-Th magma batches.

For whole-pumice geochemistry, Figures 8 and 9 clearly demonstrate, firstly, that the high and low-Th magmas are distinct with respect to both major and trace elements. Secondly, these figures indicate that Mills' (1991) XRF and INAA whole-pumice analysis are reproducable. Note that new geochemical analysis for the high and low-Th magma batches are consistent with Mills' (1991) analysis.

Furthermore, mineral assemblage compositions for all phases are, almost without exception, separate and distinct . Figures 10 through 13 demonstrate the compositional distinctness of all mineral phases present: magnetite, ilmenite, biotite and plagioclase. Only alkali feldspar compositions for both the high and low-Th magma batches are similar. If the

high and low-Th magmas were related by *in situ* differentiation, then it would be reasonable to expect mineral compositions to overlap in a manner that reflects progressive evolution of a single magma. The evidence of the compositionally distinct mineral assemblages provides additional evidence that the high and low-Th magma types are not petrogenically related by *in situ* differentiation.

Mineral chemistry and composition can provide an understanding of phase relationships, and also provide constraints on the physical conditions present in the magma chamber prior to eruption. Fortunately, the mineral assemblages for both the high and low-Th magmas were conductive to the calculation of Fe-Ti oxide and ternary-feldspar geothermometry data. Both the Fe-Ti oxide and ternary-feldspar thermometry data indicate that the high-Th magma has a consistently higher temperature than low-Th magma (Fig. 16).

The high and low-Th magma types have different whole-pumice geochemistry, different mineral compositions and different temperatures. On the basis of these fundamental and consistent distinctions, the existence of the compositionally distinct high and low-Th magma batches has been confirmed.

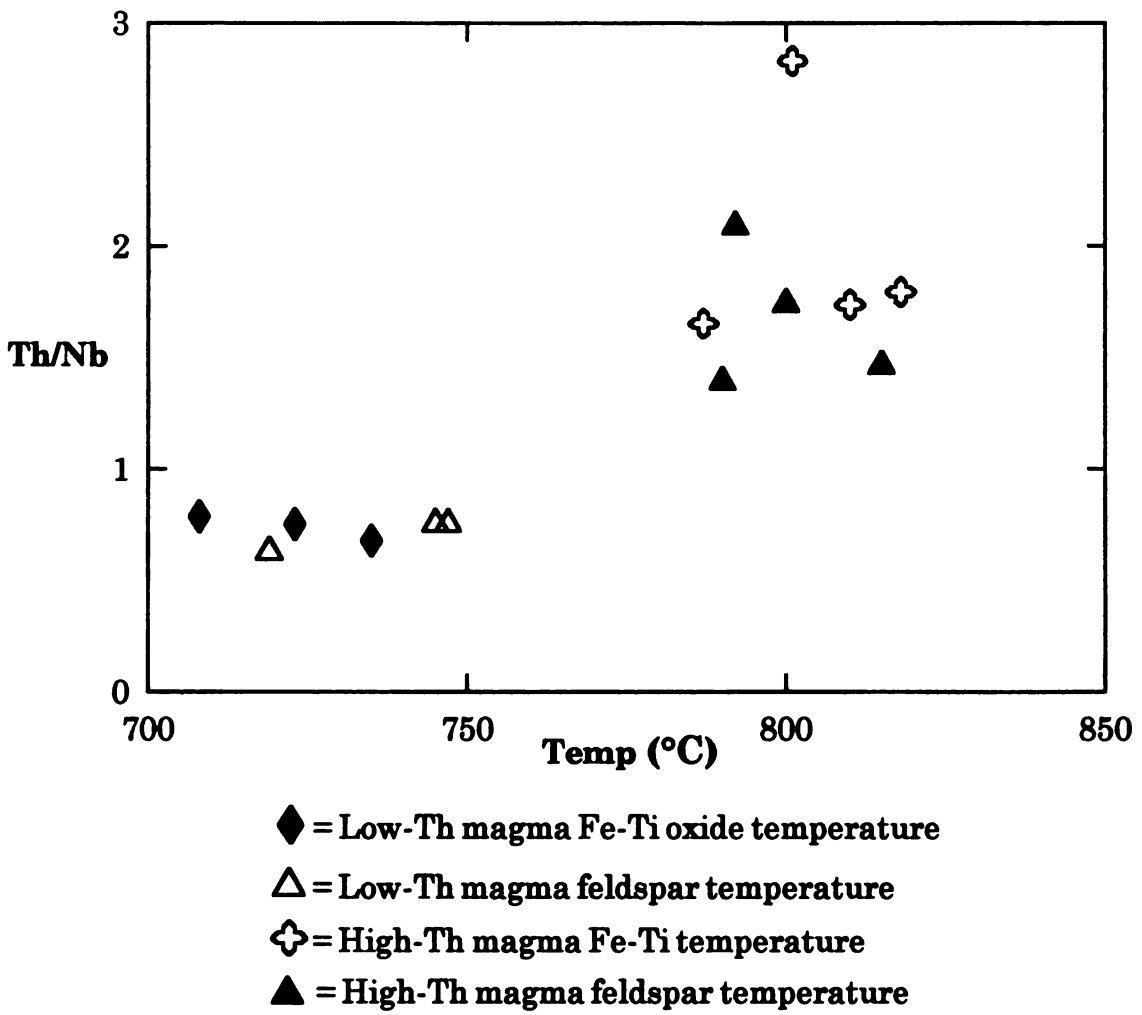

Figure 16. Temperature versus Th/Nb. Both the Fe-Ti oxide and ternary-feldspar temperature indicate that the high-Th magma had significantly higher temperatures than the low-Th magma. Furthermore, the ternary-feldspar temperature data provides confirmation of Fe-Ti oxide data.

Geothermometric Considerations

The geothermometry data establishes that the two magmas had temperature differences that ranges from 74 to 98°C. This temperature contrast implies that the surface area of contact between the high and low-Th magmas must have been relative small to prevent thermal equilibrium. Possibly, the magmas were vertically stratified in the pre-eruptive magma chamber rather than commingling as unmixed blebs prior to eruption. Vertically stratified magmas would have less contact surface area than relatively spherical pockets of coexisting magma types.

Mills (1991) evaluated the temperature distribution of the entire Rainier Mesa Tuff. His thermometry data indicates the low silica Rainier Mesa magma had temperatures which range from 875 to 900 °C. The temperatures of the low silica magma are higher than the temperatures of the high silica magmas. This observation is consistent with models of stratigraphically zoned magma chambers. These models predict that mafic magmas are overlain by cooler, less dense silicic magmas (e.g. Hildreth, 1981; Smith, 1979).

However, it should be noted that typical models of stratigraphically zoned magma chambers require *in situ* differentiation mechanisms to produce cooler, silica rich, magmas. These models, furthermore, stipulate that the temperature gradient *continuously* becomes cooler, higher in the magma chamber (Hildreth, 1981; Smith, 1979). Contrary to the conclusions

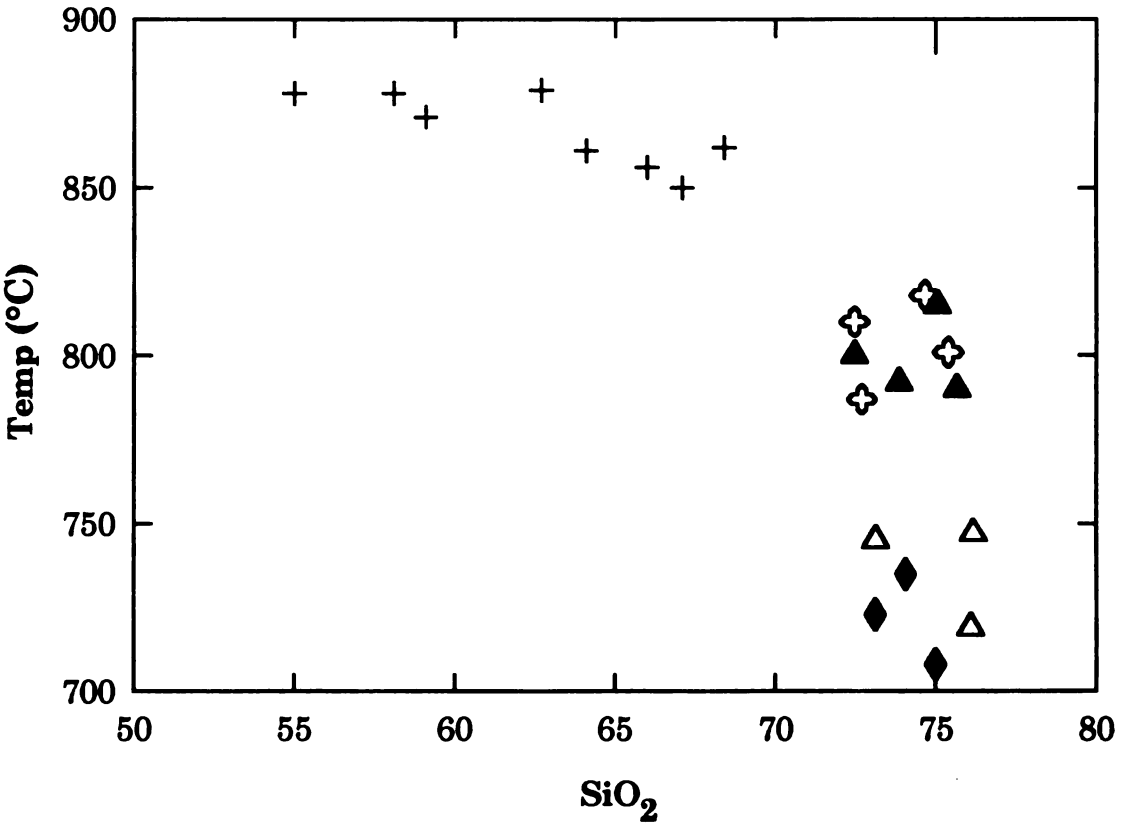

Figure 17. SiO_2 versus temperature diagram showing the discontinuous thermal gradient in the pre-eruptive Rainier Mesa magma chamber.

of Mills (1991), the pre-eruptive Rainier Mesa magma chamber had a discontinuous thermal gradient. All three of the Rainier Mesa magma types had significantly different temperatures (Fig. 17). However, it should be noted that this geothermometic data cannot preclude the existence of multiple high silica magma chambers.

In summary, geothermometric data are interpreted to indicate that the magmas in the pre-eruptive Rainier Mesa magma chamber were stratigraphically isolated rather than commingling as unmixed blebs prior to eruption. Furthermore, the presence of a discontinuous thermal gradient with sharp temperature interfaces additionally indicates that the high and low-Th magmas cannot be petrogenically related by *in situ* differentiation.

Conclusions

The purpose of this investigation was to obtain whole-pumice geochemistry and mineral assemblage chemistry to better characterize the high and low-Th magma batches and, subsequently, test the batch emplacement model of Cambray et al. (1995). The significant conclusions that resulted from this study are:

1) The existence of the high and low-Th magma batches, first observed by Mills (1991), has been confirmed. This confirmation is based on a through analysis of high and low-Th pumice geochemistry, mineral chemistry and geothermometry data. The data indicates that the two high silica Rainier Mesa magma types are chemically, mineralogically and physically distinct.

2) Fe-Ti oxide and ternary-feldspar thermometry data both indicate that the high-Th magma is hotter (≈790 °C) than the low-Th magma (≈730°C). Therefore, the contact surface area between the two magma batches must have been relatively small in order to inhibit thermal equilibrium prior to eruption of the Rainier Mesa Tuff. To minimize contact surface area, it is likely that the magmas were stratigraphically segregated and did not commingle as unmixed pockets of distinct magma.

3) The batch emplacement model of Cambray et al. (1995) is supported by this study. All step-wise multiple linear regression major element and trace element models fail to relate the high and low-Th magmas

by *in situ* differentiation mechanisms. Additionally, there are no differentiation pathways that relate the high and low-Th magmas within variation diagrams of pumice geochemistry and mineral chemistry.

4) The models of Cambray et al. (1995) and de Silva and Wolff (1995) both stipulate that *in situ* differentiation cannot produce large volume zoned magmatic systems. Because the work of Cambray et al. (1995), and consequently de Silva and Wolff (1995), has been supported by this study, the origin of many large volume compositionally zoned magmatic systems may be attributed to batch melting processes, not *in situ* differentiation.

APPENDICES

APPENDIX A

Analytical Techniques and Error Analysis

Appendix A: Analytical Techniques and Error Analysis

X-Ray Fluorescence

X-Ray Fluorescence analysis (XRF) of glassy pumice fragments provided geochemical data on all major elements and the trace elements: Cr, Ni, Cu, Zn, Rb, Sr, Y, Zr, Nb, La, and Ba. Samples were prepared for analysis by the XRF methods outlined in Mills (1991). United States Geological Survey (USGS) standards were used as both known and unknowns to determine XRF analytical error. All analytical errors for major elements are below 1%. Errors for Zn, Rb, Sr, Y, Zr, Nb are all below 10 ppm. However, La and Ba errors are greater than 10 ppm. La and Ba concentrations were resolved with greater precision using instrumental neutron activation analysis (INAA). Cr, Ni and Cu concentrations for these samples are generally below the detection limits of XRF analysis.

Instrumental Neutron Activation Analysis

All samples of the high and low-Th magma batches were analyzed by Instrumental Neutron Activation Analysis (INAA). Each sample consisted of a 0.200g to 0.250g split of the XRF powder. All samples were heat sealed in a high purity quartz tubing and sent to the Phoenix Laboratory/Ford Nuclear Reactor at the University of Michigan for extended irradiation. Sc, Hf, Th, La, Ce, Sm, Eu, Tb, Yb, and Lu concentrations were obtained by this analytical technique. INAA analysis errors for all of these elements are reported in Table 3.

Appendix A: Continued

Electron Microprobe Analysis

Phenocryst compositions were obtained by automated electron microprobe analysis on a Cameca microprobe at the University of Michigan. Phenocrysts were separated from the glassy pumice fragments using the methodology described by Mills (1991). Typically, each grain was analyzed in three localities (edge, middle and center) to determine compositional homogeneity. All minerals were analyzed with a beam current of 9.4nA at 15kV. The beam was rastered over an area of 100 um^2. Oxide and silicate standards were analyzed intermittently for calibration purposes. Furthermore, the software controlling the automated electron miroprobe analysis used the Bence-Albee correction procedure to resolve all quantitative analyses (Bence and Albee, 1968).

Table 3. Error analysis of Instrumental Neutron Activation Analysis. JG-3 is a U.S.G.S. granodiorite geostandard, and JR-2 is a U.S.G.S. rhyolite geostandard. Analytical uncertainty was calculated by determining the difference between the known and INAA predicted elemental concentrations.

	Sc	Hf	Th	La	Ce	Sm	Eu	Tb	Yb	Lu
JG-3										
Known (ppm)	8.93	4.29	8.0	20.7	41.1	3.41	0.91	0.46	1.86	0.27
Predicted (ppm)	8.40	4.45	8.5	21.8	41.2	3.32	1.01	0.64	1.47	0.20
Uncertainty (ppm)	0.53	0.16	0.5	1.1	0.1	0.09	0.10	0.22	0.39	0.07
JR-2										
Known (ppm)	5.57	5.23	32.2	16.9	38.8	5.71	0.15	1.18	5.46	0.9
Predicted (ppm)	5.38	6.22	33.9	16.5	42.9	5.34	0.20	1.21	5.40	0.9
Uncertainty (ppm)	0.19	0.99	0.7	0.4	3.9	0.37	0.05	0.03	0.06	0.0

APPENDIX B

Major and Trace Element Analyses

Appendix B: Major and Trace element analysis of the high silica Rainier Mesa Tuff. Includes data from Mills (1991). The * denotes new chemical analyses.

	Sample Number					
	R8-1	R8-2	R8-3	R8-6	R8-7	R8-9
Weight Percent Oxide (wt%)						
SiO_2	76	75.99	75.75	75.86	76.3	75.48
TiO_2	0	0.11	0.1	0.11	0.11	0.1
Al_2O_3	12	12.03	11.89	12.09	12	12.09
FeO	0	0.52	0.55	0.44	0.58	0.52
MnO	0	0.07	0.06	0.07	0.06	0.07
MgO	0	0	0	0	0	0.01
CaO	0	0.4	0.48	0.42	0.48	0.43
Na_2O	3	2.91	2.52	3.08	2.52	2.69
K_2O	5	5.34	5.69	5.16	5.7	5.54
P_2O_5	0	0.01	0.01	0.01	0.01	0.01
Total	97	97.38	97.05	97.24	97.76	96.94
X-Ray Fluorescence (ppm)						
Cr	14	7.1	0.5	10.7	12.8	7.3
Ni	0	0	1.9	0	10	0
Cu	0	10.8	0	0	0	0
Zn	30	34.3	16.3	36.1	14.8	28.3
Rb	265	258.56	264.8	257.16	271.9	266.5
Sr	3	0	4.55	0.19	0	4.96
Y	30	33.38	31.32	31.28	26.01	32
Zr	69	89.26	73.64	78.21	80.16	70.78
Nb	29	25.72	26.26	29.57	23.85	30.25
La	35	20.14	41.66	48.36	28.14	22.19
Ba	132	100	190	86	169	87
INAA (ppm)						
Sc	4	4.25	4.17	4.14	3.34	4.59
Hf	4	3.9	3.44	2.62	2.31	2.9
Th	25	25.22	21.8	16.64	11.69	15.58
La	21	21.1	21.34	19.64	20.32	24.11
Ce	51	58.68	48.81	44.91	36.33	40.07
Sm	6	6.26	5.77	5.51	5.22	5.5
Eu	0	0.18	0.17	0.14	0.19	0.2
Tb	1	0.63	0.61	0.56	0.52	0.55
Yb	4	3.54	2.81	2.87	1.67	2.15
Lu	0	0.36	0.3	0.32	0.24	0.26

Appendix B: Major and Trace element analysis of the high silica Rainier Mesa Tuff. Includes data from Mills (1991). The * denotes new chemical analyses.

	Sample Number					
	R8-10	R8-11	R8-14	R8-15	R8-16	R8-32A
	Weight Percent Oxide (wt%)					
SiO_2	74.69	73.93	75.54	75.45	73.77	73.09
TiO_2	0.09	0.09	0.1	0.1	0.12	0.21
Al_2O_3	12.2	12.48	12.21	12.16	12.86	12.84
FeO	0.42	0.39	0.42	0.46	0.74	0.86
MnO	0.07	0.07	0.07	0.07	0.08	0.05
MgO	0	0	0.04	0	0.52	0.12
CaO	0.4	0.44	0.41	0.43	0.41	0.79
Na_2O	3.48	3.54	2.73	2.52	2.51	2.82
K_2O	5.04	5.05	5.41	5.83	4.92	5.85
P_2O_5	0.01	0.01	0.01	0.01	0.02	0.03
Total	96.4	96	96.94	97.03	95.95	96.66
	X-Ray Fluorescence (ppm)					
Cr	0	0	1.4	0	2.9	7.1
Ni	0	7.4	6.6	0	13	18.9
Cu	0	0	0	0	0	0
Zn	26.8	16.9	15.9	18.5	186.8	11.3
Rb	255.72	259.5	261.78	281.95	252.21	116.65
Sr	3.65	3.48	0	0	14.09	74.99
Y	32.1	29.77	31.56	28	45.77	16.95
Zr	59.8	62.01	71.89	72.43	107.22	168.08
Nb	27.96	26.77	27.61	24.32	26.24	14.09
La	44.95	16.44	15.24	9.33	35.86	82.39
Ba	88	229	203	88	268	485
	INAA (ppm)					
Sc	4.21	3.76	4.11	3.44	3.56	1.81
Hf	3.29	3.35	3.5	3.27	4.02	5.78
Th	22.14	21.81	22.83	22.74	24.43	35.23
La	18.72	18.91	18.62	16.91	16.34	80.23
Ce	44.2	45.19	47.79	48.97	61.18	129.64
Sm	5.22	5.6	5.25	5.29	5.83	5.69
Eu	0.12	0.14	0.17	0.17	0.28	0.73
Tb	0.62	0.61	0.62	0.61	0.63	0.68
Yb	4.08	3.79	3.84	3.65	3.99	1.81
Lu	0.42	0.41	0.35	0.36	0.49	0.19

Appendix B: Major and Trace element analysis of the high silica Rainier Mesa Tuff. Includes data from Mills (1991). The * denotes new chemical analyses.

	Sample Number					
	R8-32B	R8-35	R8-40	R8-41	R8-42	R11-3
Weight Percent Oxide (wt%)						
SiO_2	74.22	75.62	73.53	73.54	74.19	73.97
TiO_2	0.25	0.2	0.2	0.22	0.27	0.11
Al_2O_3	12.35	11.72	12.83	12.95	12.59	12.53
FeO	1.01	0.87	0.81	0.88	1.02	0.5
MnO	0.06	0.04	0.04	0.05	0.05	0.05
MgO	0.15	0.03	0.07	0.12	0.15	0.25
CaO	0.81	0.51	0.73	0.78	0.75	0.67
Na_2O	2.67	2.18	2.83	2.61	2.86	2.41
K_2O	5.68	6.1	5.93	6.08	5.67	6.39
P_2O_5	0.03	0.02	0.03	0.03	0.03	0.02
Total	97.23	97.29	97	97.26	97.58	96.9
X-Ray Fluorescence (ppm)						
Cr	5.4	0	5.7	6.3	0	0
Ni	0	0	0	1	0	1.4
Cu	0	6.7	0	0	0	0
Zn	33.3	32.6	26.8	16.1	20.9	16.3
Rb	117.04	141.98	112.09	125.06	121.2	247.68
Sr	58.69	34.59	62.92	72.58	68.19	0.23
Y	18.1	21.34	21.25	23.85	21.1	28.76
Zr	183.27	153.51	152.99	169.47	193.7	78.5
Nb	13.22	15.09	14.96	15.85	16.39	31.28
La	74.55	79.83	76.09	82.36	89.85	0
Ba	189	157	263	454	433	0
INAA (ppm)						
Sc	1.81	1.97	1.62	1.73	1.95	3.66
Hf	5.78	4.71	4.4	4.87	5.42	3.27
Th	35.23	33.45	29.19	33.19	37.56	22.26
La	80.23	68.72	62.9	83.79	86.51	21.81
Ce	129.64	110.48	98.98	122.99	138.12	58.25
Sm	5.69	6.04	5.32	7.15	6.43	5.58
Eu	0.73	0.59	0.8	0.92	0.69	0.12
Tb	0.68	0.68	0.64	0.68	0.69	0.48
Yb	1.81	1.66	1.48	1.83	1.47	2.24
Lu	0.19	0.16	0.17	0.17	0.1	0.31

Appendix B: Major and Trace element analysis of the high silica Rainier Mesa Tuff. Includes data from Mills (1991). The * denotes new chemical analyses.

	Sample Number					
	R11-7	R11-20	R18-1	R18-2	R18-3	R18-4
Weight Percent Oxide (wt%)						
SiO_2	74.08	72.16	76.12	72.72	74.98	75.58
TiO_2	0.11	0.26	0.1	0.16	0.11	0.11
Al_2O_3	12.98	13.4	12.3	14.36	13.03	12.38
FeO	0.53	1.18	0.56	0.77	0.56	0.53
MnO	0.1	0.05	0.07	0.05	0.07	0.07
MgO	0.27	0.16	0.01	0.48	0.25	0
CaO	0.43	0.78	0.39	0.51	0.41	0.42
Na_2O	2.59	2.39	3.51	2.56	3.05	3.58
K_2O	6.24	7.13	4.65	5.09	5.1	4.86
P_2O_5	0.02	0.05	0.01	0.02	0.01	0.01
Total	97.35	97.56	97.72	96.72	97.57	97.54
X-Ray Fluorescence (ppm)						
Cr	0	0	0	0	0	0
Ni	13	0	0	0	0	0
Cu	0	0	0	0	0	0
Zn	8	20.1	26.9	44.1	36.4	33.5
Rb	238.42	165.9	251	155.22	238.56	252.75
Sr	4.4	97.46	1.88	10.96	0	0.47
Y	32.17	16.3	29.94	22.56	31.77	31.04
Zr	78.68	210.82	67.21	112.18	80.92	73.46
Nb	31.16	16.21	27.26	20.42	27.54	26.43
La	36.8	85.6	27.4	33.6	10.3	36.2
Ba	0	407.6	0	0	0	0
INAA (ppm)						
Sc	4.1	2.08	4.5	1.61	2.66	0.94
Hf	3.09	4.57	3.26	4.53	1.96	3.79
Th	21.11	31.26	21.44	33.72	20.88	23.29
La	23.67	82.03	26.58	31.4	16.7	31.54
Ce	60.34	135.5	42.75	79.44	48.7	47.33
Sm	5.39	6.03	5.37	5.4	5.13	5.43
Eu	0.13	0.6	0.07	0.17	0.13	0.01
Tb	0.44	0.06	0.52	0.39	0.49	0.49
Yb	2.21	1.18	2.94	2.13	1.83	2.75
Lu	0.28	0.09	0.44	0.33	0.37	0.47

Appendix B: Major and Trace element analysis of the high silica Rainier Mesa Tuff. Includes data from Mills (1991). The * denotes new chemical analyses.

	Sample Number					
	R18-5*	R18-6*	R18-8	R18-9*	R18-10*	R18-11*
Weight Percent Oxide (wt%)						
SiO_2	74.77	75	75.07	76.16	75.48	75.7
TiO_2	0.1	0.12	0.18	0.1	0.14	0.1
Al_2O_3	13.08	12.73	12.92	12.81	12.61	13
FeO	0.58	0.68	0.81	0.51	0.63	0.51
MnO	0.07	0.07	0.05	0.07	0.06	0.07
MgO	0.29	0.08	0.37	0.14	0.25	0.33
CaO	0.38	0.39	0.58	0.41	0.48	0.4
Na_2O	2.94	3.48	2.53	2.8	2.51	2.87
K_2O	5.28	4.9	5.22	5.56	5.67	5.35
P_2O_5	0.01	0.02	0.23	0.01	0.02	0.01
Total	97.5	97.47	97.96	98.57	97.85	98.34
X-Ray Fluorescence (ppm)						
Cr	46.19	50.37	0	54.04	44.58	50.68
Ni	0	0	0	0	0	0
Cu	0	0	0	0	0	0
Zn	40.94	33.47	49.6	29.83	54.15	29.71
Rb	245.06	252.29	151.73	253.55	195.36	251.54
Sr	2.03	4.73	23.87	2.69	13.65	2.93
Y	30.28	31.56	20.07	30.23	21.7	27.69
Zr	77.78	73.44	112.39	78.23	97.31	82.97
Nb	27.6	28.8	17.56	31.4	22.6	30.4
La	59.26	17.51	22	12.62	19.7	0
Ba	138.02	6.23	0	158.42	113.98	23.54
INAA (ppm)						
Sc	4.04	3.95	3.63	4	2.67	3.89
Hf	3.91	3.79	4.15	3.81	3.91	3.6
Th	24.57	22.64	34.49	23.58	29.35	23.02
La	22.55	21.15	38.23	22.03	36.43	22
Ce	51.45	50.58	88.54	51.53	72.12	48.97
Sm	4.32	4.32	5.12	4.37	5.13	4.46
Eu	0.09	0.167	0.25	0.17	0.178	0.172
Tb	0.84	0.672	0.37	0.86	0.728	0.726
Yb	3.06	3.17	2.03	3.37	2.24	3
Lu	0.513	0.527	0.26	0.52	0.337	0.495

Appendix B: Major and Trace element analysis of the high silica Rainier Mesa Tuff. Includes data from Mills (1991). The * denotes new chemical analyses.

	Sample Number					
	R18-12	R18-14*	R18-15*	R18-16	R18-18	R18-19
Weight Percent Oxide (wt%)						
SiO_2	75.11	76.1	73.13	75.42	76.22	75.41
TiO_2	0.12	0.11	0.1	0.16	0.12	0.11
Al_2O_3	12.49	12.42	12.55	12.39	12.02	12.48
FeO	0.63	0.58	0.56	0.72	0.6	0.48
MnO	0.06	0.07	0.08	0.05	0.05	0.07
MgO	0.04	0.01	0.56	0.18	0	0
CaO	0.46	0.4	1.23	0.58	0.49	0.43
Na_2O	3.41	3.47	2.75	2.93	3.36	3.53
K_2O	5.2	4.94	5.64	5.54	4.93	4.94
P_2O_5	0.01	0.01	0.01	0.02	0.01	0.01
Total	97.53	98.11	96.61	97.99	97.8	97.46
X-Ray Fluorescence (ppm)						
Cr	0	42.54	39.04	0	0	2
Ni	0	0	0	0	0	0
Cu	0	0	0	0	0	0
Zn	30.7	29.35	36.68	28	24.6	30.3
Rb	222.31	236.45	265.82	144.77	177.93	251.26
Sr	0	1.81	53.36	21.61	6.97	0
Y	25.65	33.28	26.43	18.17	19.92	27.99
Zr	83.07	70.94	87.04	109.77	87.2	71.32
Nb	21.82	33.6	29.9	11.12	15.01	23.96
La	40.9	4.86	21.74	39.6	51	22.3
Ba	0	144.94	6.5	12.8	0.9	0
INAA (ppm)						
Sc	3.5	3.59	3.83	3	3.17	3.04
Hf	3.93	3.54	3.98	3.5	3.42	3.87
Th	25.06	21.03	22.5	31.47	25.72	22.34
La	27.96	20.48	21.22	36.68	30.19	29.06
Ce	57.59	46.74	47.15	85.23	61.88	46.64
Sm	5.51	4.16	4.22	4.97	5.06	5.05
Eu	0.16	0.102	0.166	0.32	0.08	0.05
Tb	0.4	1.04	0.811	0.5	0.23	0.53
Yb	2.41	3.09	3.14	2.01	2.36	3.16
Lu	0.41	0.5	0.535	0.25	0.41	0.53

Appendix B: Major and Trace element analysis of the high silica Rainier Mesa Tuff. Includes data from Mills (1991). The * denotes new chemical analyses.

	Sample Number					
	R18-20	R18-22	R18-23	R21-5	R21-6	R21-9
Weight Percent Oxide (wt%)						
SiO_2	73.97	75	75.35	73.48	74.2	74.91
TiO_2	0.23	0.12	0.1	0.27	0.24	0.2
Al_2O_3	12.64	12.37	12.35	12.72	12.74	12.34
FeO	0.93	0.56	0.48	1.18	0.98	0.79
MnO	0.05	0.06	0.07	0.07	0.06	0.06
MgO	0.17	0	0.04	0.61	0.09	0.08
CaO	0.65	0.5	0.42	0.82	0.67	0.61
Na_2O	3.37	3.52	3.59	2.89	2.98	2.81
K_2O	5.23	5.04	5.03	5.38	5.45	5.55
P_2O_5	0.03	0.01	0.01	0.05	0.03	0.02
Total	97.27	97.18	97.44	97.47	97.44	97.37
X-Ray Fluorescence (ppm)						
Cr	0.3	0	0	1	0.4	0
Ni	0	0	0	0	0	0
Cu	0	0	0	5.4	1.1	3.5
Zn	49.3	29.7	26.9	55.9	37.8	34.6
Rb	127.58	206	253.88	99.18	111.49	122.2
Sr	45.52	6.65	5.27	66.79	59.29	31.54
Y	14.28	23.99	28.15	14.96	14.86	14.51
Zr	169.42	81.61	72.21	205.05	187.38	150.12
Nb	15.94	25.75	27.45	14.76	13.78	13.01
La	56.2	30.1	15.8	103.94	76.27	74.03
Ba	94.2	0	0	277	263	35
INAA (ppm)						
Sc	1.86	3.6	3.1	1.7	1.87	2.45
Hf	5.1	3.62	3.82	5.28	5.43	4.35
Th	33.3	26.16	21.93	32.2	34.69	31.54
La	56.73	33.34	28.81	76.52	78.5	69.46
Ce	122.61	62.65	45.59	130.81	135.81	111.06
Sm	5.99	5.17	5.26	6.63	5.76	5.38
Eu	0.54	0.03	0.03	0.59	0.6	0.4
Tb	0.3	0.37	0.42	0.74	0.74	0.75
Yb	2.16	2.64	2.98	1.84	1.85	1.86
Lu	0.32	0.42	0.55	0.18	0.25	0.24

Appendix B: Major and Trace element analysis of the high silica Rainier Mesa Tuff. Includes data from Mills (1991). The * denotes new chemical analyses.

	Sample Number					
	R21-12	R21-18	R21-19	R21-23	R21-26	R21-40
Weight Percent Oxide (wt%)						
SiO_2	74.52	75.11	74.52	74.57	75.49	76.13
TiO_2	0.21	0.14	0.13	0.13	0.13	0.13
Al_2O_3	12.21	12.13	12.63	12.41	12.09	11.99
FeO	0.85	0.72	0.72	0.69	0.71	0.61
MnO	0.05	0.08	0.08	0.08	0.08	0.05
MgO	0.34	0	0.32	0.01	0	0
CaO	0.59	0.41	0.35	0.37	0.37	0.51
Na_2O	2.54	3.55	2.99	3.75	3.6	2.88
K_2O	5.48	5.07	5.3	4.7	4.99	5.29
P_2O_5	0.03	0.01	0.01	0.01	0	0.01
Total	96.82	97.22	97.05	96.72	97.46	97.6
X-Ray Fluorescence (ppm)						
Cr	0	0	0	0	0	0
Ni	0	0	0	0	0	0
Cu	0.3	1	0	1.6	0	0
Zn	32.7	53.3	55.9	55.3	54.2	75.6
Rb	133.75	218.76	208.97	217.9	222.23	163.87
Sr	26.96	3.8	0	4.79	2.42	22.03
Y	13.94	30.06	27.64	27.16	34	15.31
Zr	166.75	131.3	128.13	120.08	125.52	95.8
Nb	12.81	28.38	28.3	31.03	31.15	18.69
La	92.15	50.51	51.7	44.27	34.22	48.65
Ba	55	0	25	128	104	134
INAA (ppm)						
Sc	1.79	1.34	1.54	1.58	1.69	2.66
Hf	5.05	5.22	3.92	5.31	5.58	2.66
Th	32.43	29.95	24.19	31.96	32.76	20.96
La	72.62	34.67	28.48	33.06	32.04	40.47
Ce	118.15	64.01	49.65	57.84	69.9	55.41
Sm	5.92	5.8	5.51	5.24	6.13	5.18
Eu	0.4	0.09	0.12	0.17	0.16	0.16
Tb	0.75	0.76	0.47	0.75	0.74	0.33
Yb	1.93	3.11	1.3	2.76	2.98	0.99
Lu	0.28	0.55	0.22	0.5	0.55	0.11

Appendix B: Major and Trace element analysis of the high silica Rainier Mesa Tuff. Includes data from Mills (1991). The * denotes new chemical analyses.

	Sample Number					
	R21-44	R21-5	R21-6	R21-9	R21-12	R21-18
	Weight Percent Oxide (wt%)					
SiO_2	74.4	73.48	74.2	74.91	74.52	75.11
TiO_2	0.24	0.27	0.24	0.2	0.21	0.14
Al_2O_3	12.83	12.72	12.74	12.34	12.21	12.13
FeO	1.06	1.18	0.98	0.79	0.85	0.72
MnO	0.05	0.07	0.06	0.06	0.05	0.08
MgO	0.13	0.61	0.09	0.08	0.34	0
CaO	0.75	0.82	0.67	0.61	0.59	0.41
Na_2O	3.03	2.89	2.98	2.81	2.54	3.55
K_2O	5.47	5.38	5.45	5.55	5.48	5.07
P_2O_5	0.03	0.05	0.03	0.02	0.03	0.01
Total	97.99	97.47	97.44	97.37	96.82	97.22
	X-Ray Fluorescence (ppm)					
Cr	11.8	1	0.4	0	0	0
Ni	0	0	0	0	0	0
Cu	0	5.4	1.1	3.5	0.3	1
Zn	45.5	55.9	37.8	34.6	32.7	53.3
Rb	116.25	99.18	111.49	122.2	133.75	218.76
Sr	69.91	66.79	59.29	31.54	26.96	3.8
Y	14.52	14.96	14.86	14.51	13.94	30.06
Zr	186.51	205.05	187.38	150.12	166.75	131.3
Nb	9.71	14.76	13.78	13.01	12.81	28.38
La	82.9	103.94	76.27	74.03	92.15	50.51
Ba	258	277	263	35	55	0
	INAA (ppm)					
Sc	1.73	1.7	1.87	2.45	1.79	1.34
Hf	3.66	5.28	5.43	4.35	5.05	5.22
Th	24.06	32.2	34.69	31.54	32.43	29.95
La	73.02	76.52	78.5	69.46	72.62	34.67
Ce	87.38	130.81	135.81	111.06	118.15	64.01
Sm	5.25	6.63	5.76	5.38	5.92	5.8
Eu	0.55	0.59	0.6	0.4	0.4	0.09
Tb	0.33	0.74	0.74	0.75	0.75	0.76
Yb	0.66	1.84	1.85	1.86	1.93	3.11
Lu	0.07	0.18	0.25	0.24	0.28	0.55

Appendix B: Major and Trace element analysis of the high silica Rainier Mesa Tuff. Includes data from Mills (1991). The * denotes new chemical analyses.

	Sample Number					
	R21-19	R21-23	R21-26	R21-40	R21-44	R23-7*
Weight Percent Oxide (wt%)						
SiO_2	74.52	74.57	75.49	76.13	74.4	72.48
TiO_2	0.13	0.13	0.13	0.13	0.24	0.29
Al_2O_3	12.63	12.41	12.09	11.99	12.83	13.65
FeO	0.72	0.69	0.71	0.61	1.06	1.36
MnO	0.08	0.08	0.08	0.05	0.05	0.06
MgO	0.32	0.01	0	0	0.13	0.44
CaO	0.35	0.37	0.37	0.51	0.75	0.85
Na_2O	2.99	3.75	3.6	2.88	3.03	2.94
K_2O	5.3	4.7	4.99	5.29	5.47	5.64
P_2O_5	0.01	0.01	0	0.01	0.03	0.05
Total	97.05	96.72	97.46	97.6	97.99	97.76
X-Ray Fluorescence (ppm)						
Cr	0	0	0	0	11.8	55.92
Ni	0	0	0	0	0	0
Cu	0	1.6	0	0	0	0
Zn	55.9	55.3	54.2	75.6	45.5	35.82
Rb	208.97	217.9	222.23	163.87	116.25	131.19
Sr	0	4.79	2.42	22.03	69.91	122.08
Y	27.64	27.16	34	15.31	14.52	26.53
Zr	128.13	120.08	125.52	95.8	186.51	250.45
Nb	28.3	31.03	31.15	18.69	9.71	20.2
La	51.7	44.27	34.22	48.65	82.9	69.63
Ba	25	128	104	134	258	485.13
INAA (ppm)						
Sc	1.54	1.58	1.69	2.66	1.73	2.13
Hf	3.92	5.31	5.58	2.66	3.66	8.04
Th	24.19	31.96	32.76	20.96	24.06	35.07
La	28.48	33.06	32.04	40.47	73.02	100.65
Ce	49.65	57.84	69.9	55.41	87.38	168.28
Sm	5.51	5.24	6.13	5.18	5.25	6.6
Eu	0.12	0.17	0.16	0.16	0.55	0.781
Tb	0.47	0.75	0.74	0.33	0.33	0.741
Yb	1.3	2.76	2.98	0.99	0.66	1.63
Lu	0.22	0.5	0.55	0.11	0.07	0.223

Appendix B: Major and Trace element analysis of the high silica Rainier Mesa Tuff. Includes data from Mills (1991). The * denotes new chemical analyses.

	Sample Number					
	R23-9*	R23-8*	R25-1	R25-11	R25-12	R25-14
Weight Percent Oxide (wt%)						
SiO_2	76.02	75.05	75.97	72.32	75.27	73.86
TiO_2	0.18	0.24	0.13	0.29	0.11	0.24
Al_2O_3	12.2	12.69	11.64	13.82	12.45	12.9
FeO	0.81	0.91	0.74	1.15	0.42	0.86
MnO	0.04	0.05	0.1	0.06	0.05	0.05
MgO	0.34	0.23	0.18	0.31	0.03	0.28
CaO	0.53	0.66	0.5	0.81	0.38	0.56
Na_2O	2.67	3.06	2.84	3.22	2.78	3.05
K_2O	5.41	5.46	5.76	5.26	5.55	5.3
P_2O_5	0.02	0.03	0.1	0.06	0.01	0.03
Total	98.22	98.38	97.96	97.3	97.05	97.13
X-Ray Fluorescence (ppm)						
Cr	39.51	48.02	0	0	1.4	0
Ni	0	0	12.4	0	0	1.7
Cu	0	0	0	0	0	0
Zn	29.38	58.07	32.8	156.8	95	108
Rb	143.44	118.85	240.85	161.35	272.61	272.23
Sr	37.31	56.71	7.45	84.66	0	47.1
Y	18.62	16.98	40.46	18.99	30.88	14.72
Zr	135.09	193.55	127.96	239.99	82.73	186.98
Nb	20.6	21.9	35	16.28	27.09	15.8
La	71.95	45.44	19.8	82.6	12.4	76.7
Ba	111.46	140.15	1.7	288	0	153.6
INAA (ppm)						
Sc	1.67	1.85	1.93	2.44	3.47	2
Hf	4.99	6.51	4.48	5.18	3.16	4.41
Th	28.14	32.02	31.12	31.59	21.75	31.22
La	48.71	75.13	33.51	93.86	23.06	70.44
Ce	94.06	129.53	79.59	156.19	57.22	125.41
Sm	4.57	5.53	6.13	6.37	5.07	5.43
Eu	0.352	0.577	0.26	0.72	0.13	0.49
Tb	0.525	0.412	0.4	0.38	0.43	0.24
Yb	1.5	1.44	2.33	1.64	2.14	1.4
Lu	0.183	0.285	0.3	0.17	0.28	0.13

Appendix B: Major and Trace element analysis of the high silica Rainier Mesa Tuff. Includes data from Mills (1991). The * denotes new chemical analyses.

	Sample Number					
	R25-16	R25-20	R26-12*	R26-14*	R26-19*	R26-20*
Weight Percent Oxide (wt%)						
SiO_2	75.68	76.07	74.98	74.67	75.67	75.1
TiO_2	0.15	0.1	0.18	0.19	0.19	0.15
Al_2O_3	12.19	12.48	12.92	12.58	12.8	12.98
FeO	0.56	0.35	0.89	0.76	0.93	0.82
MnO	0.04	0.05	0.04	0.04	0.05	0.06
MgO	0.08	0.01	0.24	0.14	0.18	0.26
CaO	0.5	0.36	0.51	0.5	0.54	0.37
Na_2O	2.77	2.94	2.38	2.77	2.45	3.16
K_2O	5.54	5.5	6	6.01	6.09	5.03
P_2O_5	0.01	0.01	0.01	0.01	0.02	0.01
Total	97.52	97.87	98.15	97.67	98.92	97.94
X-Ray Fluorescence (ppm)						
Cr	0	0	41.87	44.53	51.84	40.59
Ni	0	7	0	0	0	0
Cu	0	0	0	0	0	0
Zn	32.7	59.9	27.03	65.46	28.01	62.33
Rb	220.07	337.53	160.05	131.05	140.36	215.54
Sr	9.22	0	25.78	27.81	32.18	0
Y	25.63	28.26	19.12	19.59	20.49	34.95
Zr	104.17	68.25	131.3	144.79	150.8	95.96
Nb	17.07	28.5	22.6	17.6	21.6	29.9
La	40.9	11.4	26.42	47.88	68.18	0
Ba	0	30.8	67.07	152.27	165.88	0
INAA (ppm)						
Sc	2.47	3.88	2	1.75	1.92	4.18
Hf	3.25	2.9	4.88	5.15	5.23	4.37
Th	28.46	19.28	30.13	31.57	30	23.42
La	42.3	22.27	51.18	63.93	66.13	25.5
Ce	81.96	49.76	94.41	111.84	105.84	60.18
Sm	5.35	4.98	5.41	5.51	6.06	4.6
Eu	0.17	0.06	0.399	0.507	0.618	0.183
Tb	0.21	0.43	0.482	0.682	0.746	0.755
Yb	1.33	1.92	1.83	1.54	1.73	3.31
Lu	0.14	0.26	0.281	0.205	0.326	0.518

Appendix B: Major and Trace element analysis of the high silica Rainier Mesa Tuff. Includes data from Mills (1991). The * denotes new chemical analyses.

	Sample Number	
	R26-21*	R26-23*
Weight Percent Oxide (wt%)		
SiO_2	76.04	76.78
TiO_2	0.1	0.16
Al_2O_3	12.77	12.35
FeO	0.56	0.81
MnO	0.06	0.04
MgO	0.04	0.07
CaO	0.38	0.51
Na_2O	2.56	2.51
K_2O	6.03	5.94
P_2O_5	0.01	0.01
Total	98.55	99.18
X-Ray Fluorescence (ppm)		
Cr	42.92	37.12
Ni	0	0
Cu	0	0
Zn	18.63	23.79
Rb	260.8	150.23
Sr	0	20.3
Y	32.39	19.38
Zr	72.78	123.18
Nb	32.4	21.8
La	13.14	44.9
Ba	74.07	18.89
INAA (ppm)		
Sc	3.77	1.87
Hf	3.41	4.26
Th	22	30.45
La	22	49.59
Ce	51.12	89.52
Sm	4.57	5.25
Eu	0.153	0.361
Tb	0.766	0.536
Yb	3.65	1.65
Lu	0.568	0.312

APPENDIX C

Electron Microprobe Analyses

Appendix C: Electron Microprobe Analyses

Biotite Analysis													
descript.	F	Na_2O	MgO	Al_2O_3	SiO_2	Cl	K_2O	CaO	TiO_2	Cr_2O_3	MnO	FeO	Total
R23-14-1 edge	0.69	0.58	13.57	18.10	33.07	0.05	8.24	0.02	5.79	0.02	0.29	15.01	95.43
R23-14-1 mid	0.56	0.65	13.52	18.34	32.92	0.05	8.06	0.01	6.01	0.00	0.27	15.24	95.63
R23-14-1 ctr	0.32	0.47	13.81	18.54	32.90	0.05	8.36	0.01	5.94	0.00	0.25	15.27	95.90
R23-14-2 edge	0.63	0.68	13.61	17.84	30.99	0.02	8.23	0.02	5.98	0.00	0.27	14.93	93.21
R23-14-2 mid	0.81	0.72	14.13	18.34	36.38	0.05	8.67	0.03	5.83	0.00	0.30	15.53	100.81
R23-14-2 mid2	0.70	0.69	13.75	18.32	36.20	0.04	8.52	0.06	6.08	0.00	0.33	15.48	100.16
R23-14-3 edge	0.93	0.62	14.20	17.46	31.74	0.04	8.38	0.06	5.70	0.00	0.30	14.34	93.78
R23-14-3 mid	0.59	0.58	13.72	17.73	33.56	0.04	8.60	0.02	5.71	0.00	0.34	15.17	96.05
R23-14-3 ctr	0.77	0.64	13.93	17.67	33.74	0.03	8.44	0.02	5.71	0.00	0.28	14.85	96.08
R26-19-1 edge	1.06	0.54	13.88	16.52	36.60	0.06	8.47	0.02	4.21	0.03	0.33	15.71	97.43
R26-19-1 mid	0.97	0.55	13.88	17.73	36.96	0.08	8.38	0.02	4.12	0.01	0.35	15.68	98.74
R26-19-1 ctr	2.42	0.38	13.62	17.31	38.00	0.10	8.40	0.03	4.15	0.00	0.40	14.45	99.25
R26-19-2 edge	0.77	0.64	15.55	17.32	37.13	0.04	8.64	0.00	4.61	0.03	0.33	14.43	99.49
R26-19-2 mid	0.78	0.64	15.28	17.08	36.99	0.05	8.55	0.01	4.71	0.00	0.28	14.17	98.52
R26-19-3 edge	1.31	0.48	14.60	16.86	36.59	0.06	8.45	0.04	4.62	0.00	0.33	14.63	97.97
R26-19-3 mid	0.99	0.56	15.22	17.06	36.21	0.08	8.59	0.01	4.92	0.00	0.30	14.31	98.23
R26-19-3 ctr	0.94	0.53	14.83	17.10	35.96	0.05	8.31	0.03	4.73	0.00	0.26	14.01	96.75
R18-15-1 edge	2.38	0.44	14.19	13.01	37.82	0.10	9.07	0.02	3.52	0.04	0.67	16.19	97.45
R18-15-1 mid	2.25	0.40	13.82	12.94	37.52	0.09	8.66	0.04	3.51	0.04	0.62	16.04	95.94
R18-15-1 ctr	2.02	0.40	13.77	12.95	38.29	0.09	8.72	0.06	3.62	0.06	0.63	16.42	97.02
R18-15-2 edge2	2.50	0.51	14.21	13.05	37.54	0.07	9.35	0.02	3.61	0.06	0.77	16.73	98.41
R18-15-2 mid	1.74	0.52	13.81	12.71	35.97	0.09	9.12	0.00	3.59	0.02	0.60	16.41	94.59
R18-15-2 ctr	1.78	0.52	13.94	12.81	36.88	0.06	9.29	0.01	3.71	0.03	0.63	16.26	95.92
R18-15-3 mid	2.20	0.42	13.93	12.83	37.05	0.11	8.82	0.11	3.43	0.03	0.63	16.53	96.11
R18-6-1 edge	1.81	0.51	14.24	12.05	38.62	0.10	9.15	0.00	3.56	0.08	0.73	16.89	97.74

Appendix C: Electron Microprobe Analyses

Biotite Analysis													
descript.	F	Na_2O	MgO	Al_2O_3	SiO_2	Cl	K_2O	CaO	TiO_2	Cr_2O_3	MnO	FeO	Total
R18-6-1 mid	1.49	0.51	14.20	11.89	38.25	0.11	9.11	0.00	3.64	0.02	0.73	16.50	96.43
R18-6-1 ctr	1.44	0.57	14.68	12.19	39.39	0.09	9.30	0.00	3.53	0.08	0.76	16.43	98.46
R18-6-2 edge	1.84	0.51	13.81	12.08	38.60	0.09	9.16	0.06	3.58	0.00	0.76	16.94	97.42
R18-6-2 mid	1.67	0.52	14.54	12.60	39.94	0.09	9.17	0.00	3.65	0.05	0.78	16.33	99.33
R18-6-2 ctr	1.64	0.54	14.12	12.46	39.32	0.09	8.99	0.05	3.53	0.04	0.75	16.23	97.77
R18-6-3 edge	1.58	0.54	13.80	11.91	39.08	0.06	9.30	0.00	3.58	0.07	0.77	16.44	97.13
R18-6-3 mid	1.28	0.49	14.10	12.01	38.33	0.07	9.17	0.01	3.61	0.03	0.74	16.15	96.00
R18-6-3 ctr	1.89	0.49	14.24	12.15	38.29	0.07	9.15	0.00	3.58	0.01	0.77	15.80	96.45
R26-14-1 ctr	1.25	0.57	15.65	12.46	36.14	0.04	8.94	0.00	4.63	0.06	0.37	14.57	94.68
R26-14-2 edge	1.85	0.57	15.47	12.33	35.80	0.07	9.27	0.01	4.61	0.00	0.32	14.71	95.02
R26-14-2 mid	1.09	0.59	15.44	12.56	36.77	0.07	9.12	0.01	4.68	0.06	0.36	14.46	95.21
R26-14-2 ctr	1.15	0.49	15.54	12.44	36.75	0.05	9.11	0.01	4.84	0.00	0.41	14.21	94.98
R26-14-3 edge	1.29	0.42	14.98	12.61	36.52	0.08	9.08	0.02	4.44	0.02	0.44	15.50	95.40
R26-14-3 ctr	1.43	0.50	15.06	12.69	36.68	0.06	9.17	0.01	4.54	0.01	0.38	15.58	96.11
R18-15-1 edge	2.38	0.44	14.19	13.01	37.82	0.10	9.07	0.02	3.52	0.04	0.67	16.19	97.45
R18-15-1 mid	2.25	0.40	13.82	12.94	37.52	0.09	8.66	0.04	3.51	0.04	0.62	16.04	95.94
R18-15-1 ctr	2.02	0.40	13.77	12.95	38.29	0.09	8.72	0.06	3.62	0.06	0.63	16.42	97.02
R18-15-2 edge2	2.50	0.51	14.21	13.05	37.54	0.07	9.35	0.02	3.61	0.06	0.77	16.73	98.41
R18-15-2 mid	1.74	0.52	13.81	12.71	35.97	0.09	9.12	0.00	3.59	0.02	0.60	16.41	94.59
R18-15-2 ctr	1.78	0.52	13.94	12.81	36.88	0.06	9.29	0.01	3.71	0.03	0.63	16.26	95.92
R18-15-3 mid	2.20	0.42	13.93	12.83	37.05	0.11	8.82	0.11	3.43	0.03	0.63	16.53	96.11
R18-11-1 edge	1.80	0.66	12.31	12.68	40.66	0.08	7.19	0.28	3.16	0.04	0.61	15.64	95.10
R18-11-1 mid	1.71	0.68	12.53	13.03	39.79	0.10	7.55	0.28	3.25	0.01	0.54	14.98	94.43
R18-11-1 ctr	1.90	0.55	12.94	12.33	39.45	0.12	7.62	0.35	3.23	0.03	0.55	14.87	93.95
R18-11-2 edge	1.95	0.44	13.53	12.54	36.93	0.08	8.62	0.22	3.42	0.03	0.62	15.48	93.85

Appendix C: Electron Microprobe Analyses

Biotite Analysis													
descript.	F	Na_2O	MgO	Al_2O_3	SiO_2	Cl	K_2O	CaO	TiO_2	Cr_2O_3	MnO	FeO	Total
R18-11-2 mid	1.68	0.46	13.63	12.51	37.93	0.08	8.01	0.24	3.26	0.04	0.53	14.95	93.33
R18-11-2 ctr	1.76	0.36	13.74	12.59	38.35	0.10	8.20	0.17	3.50	0.00	0.53	15.14	94.44
R18-11-3 edge	2.59	0.48	13.88	13.05	38.05	0.06	8.72	0.22	3.45	0.00	2.36	15.60	98.46
R18-11-3 mid	1.65	0.58	13.17	12.78	38.79	0.07	8.01	0.24	3.18	0.04	0.65	15.72	94.89
R23-7-1 edge2	0.45	0.71	14.46	13.77	34.71	0.00	8.41	0.00	5.60	0.00	0.27	13.93	93.67
R23-7-1 edge3	0.74	0.49	14.73	13.87	35.38	0.02	8.45	0.00	5.23	0.02	0.30	14.20	94.69
R23-7-1 mid	0.36	0.53	14.66	13.67	35.28	0.02	8.40	0.00	5.21	0.00	0.28	14.14	93.75
R23-7-1 mid	1.72	0.60	14.57	13.95	35.51	0.09	8.71	0.13	5.63	0.13	0.40	14.48	97.72
R23-7-1 ctr	0.57	0.61	15.09	14.08	35.82	0.06	8.59	0.13	5.45	0.12	0.40	14.10	96.74
R23-7-1 edge4	0.86	0.79	15.24	14.46	35.81	0.09	8.46	0.16	5.85	0.15	0.46	13.91	98.15
R23-7-2 edge	0.76	0.67	14.65	13.47	36.14	0.10	8.86	0.21	5.73	0.14	0.51	14.83	97.12
R23-7-2 mid	0.66	0.69	14.53	13.62	35.96	0.09	9.01	0.19	5.79	0.11	0.49	14.83	97.14
R23-7-2 ctr	0.84	0.52	14.95	13.91	36.45	0.08	8.97	0.20	5.47	0.14	0.50	15.26	98.47
R23-7-3 edge	1.46	0.60	15.13	13.52	36.54	0.10	8.90	0.14	5.49	0.12	0.53	14.39	97.77
R23-7-3 mid	0.65	0.57	15.17	13.15	36.06	0.10	9.07	0.14	5.34	0.13	0.48	14.73	96.36
R23-7-3 ctr	1.45	0.58	14.96	13.14	36.43	0.08	8.96	0.15	5.42	0.14	0.55	14.74	97.41
R23-8-1 edge	1.21	0.57	15.52	12.65	36.61	0.06	9.23	0.00	4.73	0.00	0.28	14.19	95.21
R23-8-1 ctr	0.85	0.63	15.62	12.69	36.52	0.05	8.71	0.09	4.62	0.01	0.31	13.76	93.99
R23-8-2 edge	1.52	0.49	14.61	12.32	36.56	0.07	8.82	0.01	4.41	0.00	0.32	13.82	93.02
R23-8-2 ctr	1.39	0.44	14.72	13.58	35.04	0.07	8.46	0.08	5.27	0.00	0.35	14.75	95.98
R23-8-2 mid	0.85	0.49	14.98	13.51	35.45	0.07	8.76	0.01	5.34	0.00	0.38	15.36	96.71
R23-8-3 edge	1.01	0.66	16.54	13.14	38.25	0.06	9.03	0.00	4.52	0.00	0.30	13.97	97.58
R23-8-3 mid	1.12	0.40	15.84	12.76	37.75	0.07	9.26	0.00	4.44	0.00	0.27	14.53	96.50
R18-14-1 edge	2.11	0.49	14.36	13.63	37.99	0.07	8.65	0.03	3.58	0.00	0.71	16.84	98.55
R18-14-1 ctr3	1.70	0.38	12.83	13.22	38.68	0.09	7.65	0.22	3.07	0.00	0.52	14.75	93.20

Appendix C: Electron Microprobe Analyses

Biotite Analysis													
descript.	F	Na_2O	MgO	Al_2O_3	SiO_2	Cl	K_2O	CaO	TiO_2	Cr_2O_3	MnO	FeO	Total
R18-14-2 edge	1.79	0.42	14.79	12.74	37.73	0.10	9.27	0.03	3.13	0.00	0.68	16.14	96.81
R18-14-2 ctr	1.96	0.47	14.88	13.42	38.10	0.09	9.18	0.02	3.53	0.00	0.65	16.25	98.61
R18-14-3 edge	1.52	0.30	12.45	13.41	39.76	0.07	7.50	0.26	3.05	0.00	0.51	14.19	93.04
R18-14-4 edge	1.86	0.57	14.35	13.34	38.02	0.14	8.78	0.02	3.33	0.12	0.75	15.88	97.70
R18-14-4 ctr	2.08	0.58	14.60	13.17	37.33	0.13	9.29	0.00	3.44	0.13	0.90	16.39	98.60
R18-14-5 edge	1.86	0.52	13.73	12.45	35.67	0.15	9.22	0.00	3.59	0.14	0.95	16.30	95.10
R18-14-5 ctr	1.88	0.66	13.55	12.88	38.76	0.10	8.08	0.19	3.44	0.17	0.68	15.08	95.97
R18-14-5 mid	1.93	0.40	13.40	12.52	38.92	0.15	8.16	0.22	3.21	0.10	0.73	15.59	95.88

Appendix C: Electron Microprobe Analyses

Feldspar Analysis										
descript.	Na_2O	SiO_2	Al_2O_3	MgO	K_2O	CaO	BaO	FeO	Fe_2O_3	Total
R23-7-1 ctr	4.08	67.48	19.08	0.01	10.64	0.26	0.00	0.09	0.10	101.66
R23-7-1 edge	4.16	67.56	19.14	0.00	10.58	0.27	0.00	0.06	0.06	101.83
R23-7-1 mid	3.91	65.67	18.76	0.00	10.62	0.31	0.03	0.06	0.06	99.42
R23-7-2 edge	8.19	63.95	22.39	0.00	1.65	3.92	0.00	0.23	0.26	100.35
R23-7-2 mid	8.35	63.48	22.30	0.01	1.66	3.95	0.00	0.25	0.28	100.05
R23-7-2 ctr	8.16	63.58	22.64	0.00	1.52	4.36	0.00	0.18	0.20	100.46
R23-7-3 edge	4.05	65.80	18.68	0.01	10.34	0.30	0.03	0.13	0.15	99.41
R23-7-3 mid	4.11	66.76	18.92	0.01	10.41	0.28	0.08	0.03	0.04	100.64
R23-7-3 ctr	4.15	66.49	18.76	0.01	10.43	0.27	0.06	0.09	0.10	100.34
R23-8-1 edge	4.48	63.31	18.03	0.00	10.20	0.28	0.00	0.05	0.06	96.46
R23-8-1 edge	4.19	66.12	18.65	0.02	10.30	0.29	0.00	0.10	0.11	99.69
R23-8-1 mid	4.21	65.77	18.61	0.01	10.40	0.29	0.00	0.13	0.15	99.48
R23-8-1 ctr	4.10	65.87	18.50	0.00	10.57	0.30	0.00	0.05	0.06	99.46
R23-8-2 mid	8.34	62.94	22.54	0.01	1.50	4.10	0.01	0.22	0.25	99.67
R23-8-2 ctr	8.51	63.86	22.17	0.01	1.60	3.89	0.00	0.21	0.23	100.29
R23-8-3 edge	8.41	62.78	22.79	0.02	1.41	4.46	0.00	0.24	0.26	100.10
R23-8-3 mid	8.17	62.52	22.70	0.03	1.39	4.43	0.00	0.27	0.30	99.52
R23-8-3 ctr	8.27	62.25	22.58	0.01	1.40	4.57	0.00	0.30	0.34	99.39
R23-8-3 edge2	8.27	62.44	22.78	0.01	1.33	4.52	0.00	0.29	0.32	99.67
R23-4-1 mid	3.95	64.25	18.44	0.00	10.78	0.23	0.10	0.11	0.12	98.02
R23-4-1 edge	3.98	64.68	18.41	0.00	9.97	0.21	0.10	0.09	0.10	97.44
R23-4-1 edge2	4.28	65.16	18.11	0.00	9.60	0.48	0.10	0.07	0.08	97.80
R23-4-1 ctr	3.97	65.22	18.50	0.00	10.21	0.26	0.14	0.11	0.12	98.43

Appendix C: Electron Microprobe Analyses

Feldspar Analysis										
descript.	Na_2O	SiO_2	Al_2O_3	MgO	K_2O	CaO	BaO	FeO	Fe_2O_3	Total
R23-4-2 edge2	7.23	58.48	23.60	0.01	1.03	6.45	0.07	0.30	0.34	97.20
R23-4-2 mid	6.96	57.75	24.61	0.02	0.79	7.25	0.22	0.29	0.32	97.91
R23-4-2 edge	8.19	62.52	22.38	0.00	1.49	4.07	0.00	0.23	0.26	98.92
R23-4-3 mid	8.08	62.63	22.61	0.00	1.33	4.42	0.00	0.21	0.23	99.29
R23-4-3 ctr	8.25	62.60	22.32	0.00	1.42	4.23	0.01	0.28	0.32	99.14
R23-4-4 edge	6.56	56.80	26.61	0.01	0.53	8.10	0.25	0.28	0.31	99.16
R23-4-4 ctr	6.27	56.88	26.27	0.01	0.47	8.46	0.07	0.32	0.35	98.78
R18-14-1 edge	8.90	63.46	21.19	0.01	1.24	3.05	0.05	0.13	0.15	98.05
R18-14-1 mid	9.33	62.49	21.01	0.02	1.42	2.74	0.00	0.17	0.18	97.20
R18-14-1 ctr	9.42	62.91	21.17	0.00	1.27	2.95	0.00	0.16	0.17	97.89
R18-14-2 edge	3.86	63.19	17.80	0.00	10.76	0.21	0.00	0.11	0.12	95.95
R18-14-2 ctr	4.13	63.12	18.20	0.00	10.80	0.25	0.00	0.04	0.04	96.53
R18-14-2 mid	4.09	65.70	18.34	0.00	10.78	0.17	0.00	0.09	0.10	99.19
R18-14-3 edge	3.91	65.85	17.70	0.00	10.80	0.23	0.00	0.12	0.13	98.62
R18-14-3 ctr	4.06	66.08	18.43	0.00	10.81	0.17	0.00	0.11	0.12	99.65
R26-14-1 ctr	4.35	65.68	18.51	0.01	10.07	0.51	0.01	0.14	0.15	99.30
R26-14-1 mid	4.14	65.29	18.47	0.00	10.61	0.30	0.07	0.16	0.17	99.06
R26-14-2 mid	3.82	64.23	17.94	0.02	10.76	0.30	0.00	0.14	0.16	97.24
R26-14-2 ctr	3.98	64.83	17.97	0.00	10.56	0.23	0.00	0.21	0.23	97.80
R18-11-1 ctr	3.93	64.51	17.92	0.01	11.06	0.20	0.00	0.12	0.13	97.75
R18-11-2 mid	3.91	63.95	18.19	0.00	10.96	0.18	0.00	0.14	0.15	97.35
R18-11-2 ctr	4.01	64.68	18.24	0.01	10.69	0.14	0.00	0.09	0.10	97.87
R18-11-3 mid2	3.79	63.27	17.82	0.01	10.74	0.20	0.00	0.07	0.08	95.89

Appendix C: Electron Microprobe Analyses

Feldspar Analysis										
descript.	Na_2O	SiO_2	Al_2O_3	MgO	K_2O	CaO	BaO	FeO	Fe_2O_3	Total
R18-6-1 edge	8.93	65.34	20.34	0.00	1.68	2.37	0.00	0.06	0.07	98.73
R18-6-1 ctr	9.00	64.72	21.66	0.00	1.25	3.09	0.00	0.08	0.09	99.82
R18-6-1 mid	9.00	62.86	21.44	0.00	1.28	3.07	0.00	0.10	0.11	97.77
R18-6-2 mid	9.08	63.80	21.36	0.00	1.18	2.89	0.07	0.07	0.08	98.46
R18-6-2 ctr	9.31	64.37	21.15	0.00	1.28	2.82	0.01	0.11	0.12	99.08
R18-6-3 edge	7.55	59.43	23.14	0.00	0.63	5.65	0.02	0.06	0.07	96.50
R18-6-3 ctr	8.46	62.86	22.08	0.00	0.98	3.98	0.05	0.16	0.18	98.59
R18-6-3 edge2	7.80	59.06	24.65	0.00	0.52	6.40	0.00	0.13	0.14	98.57
R18-6-4 ctr	9.25	63.90	21.34	0.00	1.32	2.88	0.00	0.08	0.09	98.79
R18-6-4 edge	9.14	63.90	21.59	0.00	1.29	3.03	0.00	0.09	0.10	99.06
R26-19-1 edge2	4.13	65.37	18.21	0.00	10.52	0.31	0.09	0.17	0.19	98.82
R26-19-1 mid	4.06	65.12	18.12	0.00	10.53	0.30	0.18	0.15	0.17	98.47
R26-19-1 ctr	4.03	65.12	18.27	0.00	10.57	0.32	0.16	0.20	0.23	98.68
R26-19-2 edge	8.44	62.76	22.90	0.01	1.31	4.54	0.00	0.25	0.28	100.24
R26-19-2 mid	8.41	62.70	22.63	0.00	1.38	4.28	0.00	0.21	0.23	99.65
R26-19-2 ctr	8.17	60.87	21.93	0.00	1.44	4.06	0.04	0.24	0.27	96.77
R26-19-3 edge	4.21	64.95	18.59	0.00	10.58	0.33	0.10	0.14	0.16	98.91
R26-19-3 mid	4.10	64.89	18.36	0.00	10.54	0.34	0.10	0.13	0.15	98.48
R26-19-3 ctr	4.17	64.87	18.45	0.00	10.59	0.30	0.11	0.15	0.17	98.66
R18-9-1 mid2	4.04	65.22	18.26	0.00	10.75	0.16	0.11	0.05	0.06	98.60
R18-9-1 ctr	4.14	65.44	18.17	0.00	10.62	0.16	0.04	0.12	0.13	98.71
R18-9-1 edge	4.03	65.43	18.00	0.01	10.60	0.16	0.16	0.10	0.12	98.50
R18-9-2 edge	4.04	66.44	18.16	0.02	10.46	0.16	0.16	0.11	0.12	99.57

Appendix C: Electron Microprobe Analyses

Feldspar Analysis										
descript.	Na_2O	SiO_2	Al_2O_3	MgO	K_2O	CaO	BaO	FeO	Fe_2O_3	Total
R18-9-2 ctr	4.18	65.34	18.52	0.00	10.56	0.13	0.09	0.10	0.11	98.94
R18-9-3 edge	8.82	62.57	20.92	0.00	1.33	2.75	0.00	0.19	0.21	96.59
R18-9-3 ctr	9.21	63.50	21.23	0.00	1.27	2.77	0.00	0.13	0.15	98.13
R18-9-3 mid	9.13	63.62	20.75	0.01	1.29	2.75	0.00	0.16	0.17	97.73
R18-15-1 edge	4.02	65.45	18.40	0.01	10.86	0.15	0.00	0.06	0.07	98.96
R18-15-1 mid	4.10	65.89	18.46	0.00	10.93	0.14	0.06	0.12	0.14	99.72
R18-15-1 ctr	4.02	66.19	18.37	0.00	10.74	0.15	0.00	0.10	0.11	99.59
R18-15-2 edge	4.12	66.47	18.52	0.00	10.76	0.14	0.00	0.04	0.05	100.06
R18-15-2 mid	4.04	66.41	18.58	0.00	10.85	0.12	0.01	0.04	0.05	100.07
R18-15-2 ctr	4.11	65.81	18.60	0.00	10.77	0.15	0.00	0.01	0.01	99.46
R18-15-3 edge	9.17	65.71	21.03	0.00	1.34	2.70	0.00	0.11	0.12	100.08
R18-15-3 mid	9.29	65.59	21.17	0.00	1.35	2.80	0.00	0.13	0.14	100.34
R18-15-4 edge	3.95	63.59	18.13	0.00	10.69	0.14	0.00	0.05	0.06	96.56
R18-15-4 mid	4.11	65.72	18.43	0.00	10.78	0.13	0.06	0.08	0.09	99.32
R18-15-5 edge	4.07	66.18	18.54	0.00	10.81	0.12	0.01	0.07	0.08	99.80
R18-15-5 ctr	4.02	66.31	18.49	0.01	10.85	0.17	0.00	0.04	0.05	99.89

Appendix C: Electron Microprobe Analyses

Magnetite Analysis							
descrip.	MgO	Al_2O_3	TiO_2	Cr_2O_3	MnO	FeO	Total
R18-15-2 mid	0.57	0.99	4.71	0.04	2.06	84.78	93.18
R18-15-2 ctr	0.58	0.97	4.68	0.01	2.13	84.77	93.20
R18-15-3 edge	0.22	1.12	4.84	0.00	1.24	82.69	90.18
R18-15-3 ctr	0.46	0.89	4.81	0.00	2.15	84.48	92.86
R23-7-1 edge	0.84	1.23	6.67	0.01	0.98	82.39	92.32
R23-7-1 ctr	0.22	0.95	7.25	0.11	0.31	79.43	88.80
R23-7-2 edge	1.03	2.11	4.99	0.05	0.91	65.79	80.21
R23-7-2 edge2	1.54	2.19	5.46	0.06	1.36	81.52	92.39
R23-7-2 ctr	1.13	1.83	7.19	0.03	0.95	81.33	92.67
R18-6-1 mid	0.26	1.30	5.33	0.16	1.54	83.22	91.99
R18-6-1 mid2	0.16	0.95	5.03	0.11	1.37	84.28	92.02
R18-6-1 ctr	0.16	1.11	5.08	0.14	1.33	83.82	93.49
R18-6-2 edge	0.30	1.08	5.08	0.13	1.50	84.56	92.77
R18-6-2 mid	0.41	0.81	4.98	0.13	2.39	84.74	93.65
R18-6-2 ctr	0.51	1.05	4.94	0.14	2.57	84.59	93.97
R18-6-3 edge	0.39	0.88	4.79	0.11	2.52	84.63	93.44
R18-6-3 ctr	0.34	1.11	5.07	0.15	1.74	83.79	92.31
R26-14-1 edge	0.93	1.06	6.05	0.04	1.08	80.99	90.38
R26-14-1 mid	0.94	0.95	5.61	0.00	1.12	83.75	92.44
R26-14-2 edge	0.41	2.14	6.59	0.07	0.78	76.86	90.56
R26-14-2 mid	1.09	1.32	5.34	0.09	1.53	83.30	92.82
R18-15-2 mid	0.57	0.99	4.71	0.04	2.06	84.78	93.18
R18-15-2 ctr	0.58	0.97	4.68	0.01	2.13	84.77	93.20
R18-15-3 edge	0.22	1.12	4.84	0.00	1.24	82.69	90.18
R18-15-3 ctr	0.46	0.89	4.81	0.00	2.15	84.48	92.86
R23-7-1 edge	0.84	1.23	6.67	0.01	0.98	82.39	92.32
R23-7-1 ctr	0.22	0.95	7.25	0.11	0.31	79.43	88.80
R23-7-2 edge	1.03	2.11	4.99	0.05	0.91	65.79	80.21

Appendix C: Electron Microprobe Analyses

Magnetite Analysis							
descrip.	MgO	Al_2O_3	TiO_2	Cr_2O_3	MnO	FeO	Total
R23-7-2 edge2	1.54	2.19	5.46	0.06	1.36	81.52	92.39
R23-7-2 ctr	1.13	1.83	7.19	0.03	0.95	81.33	92.67
R18-11-1 mid	0.54	0.94	4.84	0.11	2.31	84.16	93.00
R18-11-1 ctr	0.31	1.11	4.96	0.00	1.60	83.26	91.35
R18-15-1 mid	0.02	0.17	0.00	0.02	1.26	87.17	89.53
R18-15-1edge	0.00	0.38	0.00	0.00	1.11	87.72	90.00

Appendix C: Electron Microprobe Analysis

Ilmenite Analysis							
descript.	MgO	Al_2O_3	TiO_2	Cr_2O_3	MnO	FeO	Total
R23-14-1 edge	1.22	0.11	39.80	0.07	1.54	49.50	92.56
R23-14-1 mid	2.65	0.17	36.53	0.04	3.47	49.77	92.86
R23-14-1 ctr	1.31	0.18	36.48	0.06	1.67	53.06	93.06
R23-14-2 edge	1.21	0.19	42.69	0.10	3.11	44.73	92.22
R23-14-2 mid	1.20	0.09	43.43	0.06	3.49	43.69	92.19
R26-19-1 edge	1.13	0.08	38.60	0.10	1.40	53.44	94.85
R26-19-1 ctr	1.57	0.14	39.48	0.07	1.81	51.58	94.79
R26-19-2 edge	2.56	0.28	36.60	0.04	2.16	51.32	93.82
R26-19-2 mid	1.75	0.18	38.00	0.16	1.41	53.83	95.41
R26-19-2 ctr	0.93	0.22	37.54	0.08	0.85	53.81	93.54
R26-19-3 edge	1.64	0.16	38.32	0.10	1.72	53.41	95.41
R26-19-3 ctr	1.46	0.13	38.05	0.13	1.65	53.92	95.38
R23-7-1 edge	1.36	0.17	37.96	0.00	1.10	52.60	93.34
R23-7-1mid	2.32	0.15	36.75	0.05	2.00	53.82	95.14
R23-7-1ctr	2.16	0.16	36.83	0.01	1.75	53.96	94.88
R23-7-2 edge	1.76	0.15	37.40	0.00	1.55	53.68	94.58
R23-7-2 mid	2.41	0.18	36.85	0.00	1.86	53.54	94.88
R23-7-2 ctr	2.18	0.17	37.01	0.02	1.94	53.93	95.29
R23-8-1 edge2	1.17	0.11	38.56	0.09	0.84	52.89	93.77
R23-8-1 mid	1.57	0.18	37.78	0.04	1.23	53.34	94.21
R23-8-1 ctr	2.07	0.11	37.45	0.02	1.39	52.57	93.77
R23-8-2 edge	0.76	0.16	38.37	0.02	0.67	52.07	92.24
R23-8-2 mid	0.87	0.18	36.80	0.00	0.61	55.08	93.69
R23-8-2 ctr	1.15	0.12	38.33	0.01	0.89	52.80	93.47
R23-8-3 edge	1.53	0.15	38.45	0.00	1.14	52.05	93.42
R23-8-3 mid	1.98	0.14	38.98	0.04	1.60	51.30	94.26
R23-8-3ctr	0.62	0.21	38.03	0.00	0.40	53.73	93.20
R18-6-1 edge	0.61	0.00	44.86	0.11	2.71	47.82	96.25

Appendix C: Electron Microprobe Analysis

Ilmenite Analysis							
descript.	MgO	Al_2O_3	TiO_2	Cr_2O_3	MnO	FeO	Total
R18-6-1 mid	1.09	0.00	44.41	0.10	4.75	48.40	98.85
R18-6-1 ctr	1.28	0.01	43.77	0.09	4.87	47.65	97.81
R18-6-2 edge	0.49	0.03	45.01	0.14	2.26	47.59	95.64
R18-6-2 mid	1.16	0.01	43.89	0.09	4.68	48.12	98.07
R18-6-2 ctr	1.20	0.00	43.95	0.12	4.91	47.84	98.13
R18-6-3 edge	0.63	0.00	45.08	0.07	2.89	46.61	95.43
R18-6-3 mid	1.10	0.00	43.93	0.10	6.10	45.49	96.86
R26-14-1 edge	2.33	0.08	38.51	0.08	2.49	51.67	95.32
R26-14-1 mid	2.30	0.06	38.72	0.10	2.22	52.39	95.90
R26-14-2 edge	1.20	0.09	38.66	0.13	1.20	52.77	94.12
R26-14-2 ctr	2.08	0.09	38.07	0.04	2.23	53.26	95.94
R23-7-1edge	1.36	0.17	37.96	0.00	1.10	52.60	93.34
R23-7-1mid	2.32	0.15	36.75	0.05	2.00	53.82	95.14
R23-7-1ctr	2.16	0.16	36.83	0.01	1.75	53.96	94.88
R23-7-2 edge	1.76	0.15	37.40	0.00	1.55	53.68	94.58
R23-7-2 mid	2.41	0.18	36.85	0.00	1.86	53.54	94.88
R23-7-2 ctr	2.18	0.17	37.01	0.02	1.94	53.93	95.29
R18-11-1 mid	1.14	0.09	43.22	0.00	4.25	47.11	95.89
R18-11-1 edge	1.20	0.07	42.95	0.00	4.69	47.15	96.14
R18-11-2 mid	0.98	0.10	43.47	0.00	3.83	47.33	95.77
R18-15-1 mid	1.50	0.05	43.47	0.00	5.35	45.07	95.53
R18-15-1 ctr	1.42	0.04	42.82	0.00	6.19	45.16	95.68
R18-15-1 edge	1.06	0.04	42.77	0.00	3.82	48.19	95.92
R18-15-2 mid	1.12	0.08	42.34	0.00	4.08	47.22	94.97
R18-15-2 ctr	1.01	0.07	42.80	0.01	4.36	47.98	96.34
R18-15-3 edge	1.08	0.07	44.10	0.01	3.55	46.04	94.97
R18-15-3 ctr	1.56	0.09	43.86	0.00	5.47	45.09	96.09

BIBLIOGRAPHY

BIBLIOGRAPHY

Anderson, D.J., Lindsley, D.H., and Davidson, P.M., 1993. QUILF; a pascal program to assess equilibria among Fe-Mg-Mn-Ti oxides, pyroxenes, olivine, and quartz. Computers and Geosciences, v.19, p.1333-1350.

Aramaki, S., and Lipman, P.W., 1965. Possible leaching of Na_2O during hydration of volcanic glasses. Japan Acadamy Proceedings, v. 41, p. 41-47.

Bence, A.E., and Albee, A.L., 1968. Empirical correction factors for the electron microanalysis of silicates and oxides. Journal of Geology, v. 76, p. 382-403.

Best, M.G., Christiansen, E.H. and Blank, R.H., 1989. Oligocene caldera complex and calc-alkaline tuffs and lavas of the Indian Peak volcanic field, Nevada and Utah. Bulletin of the Geological Society of America, v. 101, p. 1076-1090.

Brown, W.L., and Parsons, I., 1981. Towards a more practical two-feldspar geothermometer. Contributions to Mineralogy and Petrology, v. 76, p. 369-377.

Byers, F.M. Jr., Carr, W.J., Orkild, P.P., Quinlivan, W.D., and Sargent, K.A., 1976a. Volcanic suites and related cauldrons of the Timber Mountain-Oasis Valley caldera complex southern Nevada. U.S. Geological Survey Professional Paper, v. 919, 70pp.

Cambray, F.W., Vogel, T.A., Mills, J.G., Jr., 1995. Origin of compositional heterogeneities in the tuffs of the Timber Mountain Group: The relationship between magma batches and magma transfer and emplacement in an extensional environment. Journal of Geophysical Research, v. 100, no. B8, p. 15,793-15,805.

Cameron, K.L, and Cameron, M., 1986. Whole-rock/groundmass differentiation trends of rare earth elements in high-silica rhyolites. Geochimica et Cosmochimica Acta, v. 50, p. 759-769.

Carr, W.J., 1990. Styles of extension in the Nevada Test site region, southern Walker Lane Belt; an integration of volcano-tectonic detachment fault models. In: Wernicke, B. (Editor), Basin and Range Extensional Tectonics Near the latitude of Las Vegas, Nevada. Memoirs of the Geological Society of America, v. 176, p. 283-303.

Carrigan, C.R., 1994. Two-component magma transport and the origin of composite intrusions and lava flows. In: Ryan, M.P. (Editor), Magmatic systems. Academic, p. 319-353.

Carrigan, C.R., and Eichelberger,J.C., 1990. Zoning of magmas by viscosity in volcanic conduits. Nature, v.343, p. 248-251.

Christiansen, R.L., Lipman, P.W., Carr, W.J., Byers, F.M., Orkild, P.P., and Sargent, K.A., 1977. The Timber Mountain-Oasis Valley caldera complex of southern Nevada. Geological Society of America Bulletin, v. 88, p. 943-959.

de Silva, S.L., 1989a. The origin and significance of crystal rich inclusions in pumices from two Chilean ignimbrites. Geol. Mag., v. 126, p. 150-175.

de Silva, S.L., 1991. Styles of zoning in Central Andean ignimbrites- insights into magma chamber processes. Geological Society of America Special Paper, v. 265, p. 217-231.

de Silva, S.L., and Wolff, J.A., 1995. Zoned magma chambers: the influence of magma chamber geometry on sidewall convective fractionation. Journal of Volcanology and Geothermal Research, v. 65, p. 111-118.

Dunbar, N.W., and Herving, R.L., 1992b. Volatile and Trace Element Composition of Melt Inclusions From the Lower Bandelier Tuff: Implications for Magma Chamber Processes and Eruptive Style. Journal of Geophysical Research, v. 97, no. B11, p. 15,151-15,170.

Eaton, G.P., 1984. The Miocene Great Basin of western North America as an extending back-arc region. In: Carlson, R.L., and Kobayashi, K. (Editors), Geodynamics of back-arc regions. Tectonophysics, v. 102, p. 275-295.

Flood, T.P., 1987. Cyclic evolution of a magmatic system: The Paintbrush Tuff, Southwest Nevada Volcanic Field. Ph.D. thesis, 147pp., Michigan State University, East Lansing.

Flood, T.P., Schuraytz, B.C., and Vogel, T.A., 1989b. Magma mixing due to disruption of a layered magma body. Journal of Volcanology and Geothermal Research, v. 36, p. 241-255.

Flood, T.P., Vogel, T.A., Schuraytz, B.C., 1989a. Chemical evolution of a magmatic system: The Paintbrush Tuff, Southwest Nevada Volcanic Field. Journal of Geophysical Research, v. 94, p.5943-5960.

Fuhrman, M.L. and Lindsley, D.H., 1988. Ternary-feldspar modeling and thermometry. American Mineralogist, v. 73, p. 201-215.

Hildreth, W., 1981. Gradients in silicic magma chambers: implications for lithospheric magmatism. Journal of Geophysical Research, v. 86, p. 10,153-10,192.

Hildreth, W., and Mahood, G., 1985. Correlation of ash-flow tuffs: Geological Society of America Bulletin, v. 96, p. 968-974.

Huysken, K.T., Vogel, T.A., and Layer, P.W., 1994. Incremental growth of a large volume, chemcially zoned magma body: A study of the tephra sequence beneath the Rainier Mesa ash-flow sheet of the Timber Mountain Tuff. Bulletin of Volcanology, v. 56, p. 377-385.
in volcanic conduits. Nature, v. 343, p. 248-251.

Irvine, T.N., and Barager, W.R.A., 1971. A quick guide to the chemical classification fo common rocks. Canadian Journal of Earth Science, v. 8, p.523-548.

Le Bas, M.J., Le Maitre, R.W., Streckeisin, A., and Zanettin, B., 1986. A chemical classification of volcanic rocks based on the Total Alkai-Silica diagram. Journal of Petrology, v. 27, p. 745-750.

Lipman, P.W., 1965. Chemical comparison of glassy and crystalline volcanic rocks. Geological Society of America Special Paper, v. 82, p. 260-261.

Michael, P.J., 1983. Chemical differentiation of the Bishop Tuff and other high-silica magmas through crystallization processes. Geology, v. 11, p. 31-34.

Mills, J.G., Jr, 1991. The Timber Mountain Tuff, southwestern Nevada volcanic field: Geochemistry, mineralogy and petrogenesis. Ph.D. thesis, 332pp., Michigan State University, East Lansing.

Noble, D.C., 1967. Sodium, potassium, and ferrous iron contents of some secondarily hydrated natural silicic glasses. American Mineralogist, v. 52, p. 280-286.

Palacz, Z.A., and Wolff, J.A., 1989. Strontium, neodymium and lead isotope characteristics of the Granadilla Pumice, Tenerife: a study of the causes of strontium isotipe disequilibrium in felsic pyroclastic deposits. In: A.D. Saunders and M.J. Norry(Editors), Magmatism in the Ocean Basins. Geological Society of London Special Publication, v. 42, p. 147-159.

Sawyer, D.A., Fleck, R.J., Lanphere, M.A., Warren, R.G., Broxton, D.E., and Hudson, M.R., 1994. Episodic caldera volcanism in the Miocene southwestern Nevada volcanic field: Revised stratigraphic framework, $^{40}Ar/^{39}Ar$ geochronology, and implications for magmatism and extension. Geological Society of America Bulletin, v. 106, p. 1304-1318.

Schuraytz, B.C., Vogel, T.A., and Younker, L.W., 1989. Evidence for dynamic withdrawal from a layered magma body: The Topopah Spring Tuff, southwestern Nevada. Journal of Geophysical Research, v. 94, p. 5925-5942.

Scott, R.B., 1990. Tectonic setting of Yucca Mountain, southwest Nevada. In: Wernicke, B. (Editor), Basin and Range Extensional Tectonics Near the latitude of Las Vegas, Nevada. Memoirs of the Geological Society of America, v. 176, p.251-282.

Smith, R.L., 1979. Ash-flow magmatism. Geological Society of America Special Paper, v. 180, p.5-27.

Stewert, J.H., 1988. Tectonics of the Walker Lane belt, western Great Basin: Mesozoic and Cenozoic deformation in a zone of shear. In: Ernst, W.G. (Editor), Metamorphism and Crustal Evolution of the Western United States, Ruby v. VII, p. 683-713.

Stix, J. and Gordon, M.P., 1993. Replenishment and crystallization in epicontinental silicic magma chambers: evidence from the Bandelier magmatic system. Journal of Volcanology and Geothermal Research, v. 55, p. 201-215.

Stormer, J.C., Jr, 1975. A practical two-feldspar geothermometer. American Mineralogist, v. 60, no. 9, p. 723-726.

Tegtmeyer, K.J., and Farmer, G.L., 1990. Nd isotopic gradients in upper crustal magma chambers: evidence for *in situ* magma-wall-rock interaction. Geology, v. 18, p. 5-9.

Vogel, T.A., 1995. unpublished data.

Vogel, T.A., Mills, J.G. Jr., Aines, R.D., and Merzbacher, C.I., 1989. Pre-eruptive volatiles in a chemically zoned magma body based on melt inclusions. Geological Society of America Abstracts with Programs, v. 21, n.6, p. A271.

Vogel, T.A., Ryerson, F.J., Noble, D.C., and Younker, L.W., 1987. Limits to magma mixing based on chemistry and mineralogy of pumice fragments erupted from a chemically zoned magma body. Journal of Geology, v. 95, p.659-670.

Wen, S. and Nekvasil, H., 1994. SOLVCALC; an interactive graphics program package for calculating the ternary feldspar solvus and for two-feldspar geothermometry. Computers and Geology, v.20, p. 1025-1040.

Whitney, J.A., and Stormer, J.C., 1985. Mineralogy, petrology, and magmatic conditions from the Fish Canyon Tuff, central San Juan Volcanic Field, Colorado. Journal of Petrology, v. 26, p. 726-762.

Wolff, J.A., and Storey, M., 1984. Zoning in highly alkaline magma bodies. Geol. Mag., v. 121, p. 563-575.

Worner, G., and Schmincke, H.U., 1984a. Mineralogical and chemical zonation of the Laacher See tephra sequnce(East Eifel, FRG). Journal of Petrology, v. 25, p. 805-835.

Worner, G., and Schmincke, H.U., 1984b. Petrogenesis of the zoned Laacher See tephra. Journal of Petrology, v. 25, p. 836-851.

Worner, G., Staudigel, H., and Zindler, A., 1985. Isotopic constraints on open system evolution of the Laacher See magma chamber (Eifel, FRG). Earth and Planetary Science Letters, v. 75, p. 37-49.